International Journal of Biological Macromolecules 319 (2025) 145645

Contents lists available at ScienceDirect

International Journal of Biological Macromolecules

journal homepage: www.elsevier.com/locate/ijbiomac

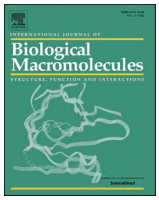

Injectable borax-loaded alginate hydrogels reduce muscle atrophy, modulate inflammation, and promote neuroprotection in the SOD1^{G93A} mouse model of ALS through mechanisms involving IGF–Akt–mTOR signaling

Ana Rodriguez-Romano [a,b,1], Juan Gonzalez-Valdivieso [b,c,1], Laura Moreno-Martinez [d,e], Juan Francisco Vázquez Costa [f,g], Rosario Osta [d,e], Patricia Rico [a,b,*]

[a] Biomedical Research Networking Center in Bioengineering, Biomaterials and Nanomedicine (CIBER-BBN), Spain
[b] Center for Biomaterials and Tissue Engineering (CBIT), Universitat Politècnica de València, 46022 Valencia, Spain
[c] University of Valladolid, 47002 Valladolid, Spain
[d] Biomedical Research Networking Center in Neurodegenerative Disorders (CIBERNED), Spain
[e] Laboratory of Genetics and Biochemistry (LAGENBIO), Faculty of Veterinary-IIS Aragón, IA2-CITA, University of Zaragoza, 50013 Zaragoza, Spain
[f] Biomedical Research Networking Center on Rare Diseases (CIBERER), Spain
[g] Neuromuscular Unit Hospital Universitario y Politécnico la Fe, IIS La Fe, 46026 Valencia, Spain

ARTICLE INFO

Keywords:
Borax
ALS
Muscle regeneration
NaBC1 transporter (*SLC4A11*)
Alginate hydrogel

ABSTRACT

Amyotrophic Lateral Sclerosis (ALS) is a prevalent condition characterized by motor neuron loss and skeletal muscle paralysis. Despite being associated to mutations in over 40 genes, its etiology remains elusive without a cure or effective treatment. ALS, historically considered a motor neuron disease, is defined today as a multisystem disorder involving non-neuronal cell types, including early muscle pathology independent of motor neuron degeneration (dying back hypothesis), thus skeletal muscle actively contributes to disease pathology, making it a viable therapeutic target for ALS.

Our previous research has shown that boron transporter NaBC1 (encoded by the *SLC4A11* gene), after activation co-localizes with integrins and growth factor receptors synergistically enhancing muscle repair. Here we investigate the effects of injectable alginate-based hydrogels for controlled local borax release in Amyotrophic Lateral Sclerosis muscle. Treated mice showed improved motor function, prolonged survival, and activation of essential muscle metabolic pathways, leading to enhanced muscle repair and reduced atrophy and inflammation. Interestingly, local muscle repair activation provided retrograde neuroprotection by preserving motor neurons and reducing neuro-inflammation. This study highlights the role of muscle tissue in ALS pathology, supporting its targeting with NaBC1-based therapies for muscle regeneration.

1. Introduction

Amyotrophic Lateral Sclerosis (ALS) is the most frequent and fatal motor neuron disease. [1] Although ~10 % of cases are familial, both familial and sporadic ALS exhibit indistinguishable clinical features, suggesting a convergence of diverse pathogenic pathways. Despite the identification of >40 ALS-related genes (https://alsod.ac.uk/, accessed 17 November 2024), the etiology remains largely unknown, with no cure or effective treatment available, only multidisciplinary care. [2]

The multisystemic nature of ALS, spanning various biological systems, and the high variability in clinical progression, even among patients carrying the same mutation, [3,4] further complicates the identification of a suitable therapeutic target.

While ALS is considered the prototype of motor neuron diseases, muscle weakness and degeneration are central pathological hallmarks. Accumulating evidence now defines ALS as a multisystem disorder involving changes also in non-neuronal cell types involving glial [5] and muscle cells. [6] Moreover, the 'dying back' hypothesis proposes that

* Corresponding author at: Biomedical Research Networking Center in Bioengineering, Biomaterials and Nanomedicine (CIBER-BBN), Spain.
E-mail address: parico@upvnet.upv.es (P. Rico).
[1] Equal contribution.

https://doi.org/10.1016/j.ijbiomac.2025.145645
Received 11 December 2024; Received in revised form 19 June 2025; Accepted 28 June 2025
Available online 30 June 2025

early pathological changes occur at the neuromuscular junction or distal axon, leading to a progressive degeneration of motor neurons, potentially initiated by signals from the skeletal muscle before the appearance of motor symptoms. [7,8] Skeletal muscle is increasingly recognized as an active participant in disease progression, capable of secreting trophic and inflammatory factors that influence neuromuscular integrity. Observations of early muscle pathology independent of motor neuron loss highlight its relevance as a potential therapeutic target in ALS. [9]

Therapies targeting muscle atrophy and motor neuron degeneration often employ growth factors delivered systemically, [10,11], through stem cells [12] or directly targeting muscle inflammation. [13] However, few studies explore bioactive material systems capable of delivering therapeutic ions that modulate intracellular signaling. [14–17] Still there is a need to innovate and establish new methods and materials that facilitate the repair and functional regeneration of skeletal muscle.

Ions such as calcium are involved in key signaling pathways, angiogenesis, [17] and muscle function regulation *via* calcium homeostasis under oxidative stress conditions. [18,19] Boron, essential in mammalian metabolism, [20,21] is transported by NaBC1 (*SLC4A11*), a Na^{+}-coupled borate transporter. [22] Recently our group identified NaBC1 as a mechanosensory [23] that interacts with fibronectin-binding integrins and growth factor receptors (GFR), forming functional clusters that enhance mechanotransduction and tissue regeneration processes, including angiogenesis, [24] adhesion-driven osteogenesis, [25] and muscle regeneration. [26,27]

In this study, we investigated in a local proof of concept, the therapeutic potential of borax released from injectable alginate hydrogels in the quadriceps of symptomatic $SOD1^{G93A}$ mice, a model in which muscle denervation precedes motor neuron loss. [7,28] A local regimen of four injections significantly improved motor function, delayed symptom onset, and extended survival. The treatment also reduced muscle atrophy, increased muscle satellite cell activation and enhanced myogenic and metabolic signaling involved in muscle repair processes, resulting in a decrease in muscle inflammation. Furthermore, the recovery of muscle pathology had retrograde neuroprotective effects in the spinal cord, reducing neuroinflammation and motor neuron loss. These findings highlight skeletal muscle as a central therapeutic target in ALS and propose NaBC1 activation as a novel and promising strategy for muscle regeneration in neuromuscular diseases.

2. Results and discussion

2.1. Local borax-release preserves motor function, delays evident symptoms onset, and prolongs survival in a $SOD1^{G93A}$ mouse model

In this work, we aimed to assess the effects of boron in the form of borax (B), as a local proof of concept, in an Amyotrophic Lateral Sclerosis (ALS) murine model (B6SJL-Tg ($SOD1^{G93A}$) 1 Gur/J ALS) to evaluate the possible effects of B in the recovery of the pathological conditions of muscle and nerve inflammation caused by ALS degeneration. To do that, we engineered and characterized injectable alginate-based hydrogels with controlled local B-release as previously described. [26] We loaded the hydrogels with B 0.15 M equivalent to 6 mg per 100 μL hydrogel (ALG—B). Fig. S1-a shows the non-cumulative B-release of 6 mm injectable hydrogels. Release from ALG-B hydrogels resulted in approximately 1200 mg L^{-1} at day 1 (equivalent to 20 % of B after 1 day Fig. S1-b), despite the initial loading of 6000 mg L^{-1} indicating that part of the B content remains entrapped within the hydrogel and becomes sustained released over time.

The mechanical properties of the ALG and ALG-B injectable hydrogels were evaluated by rheometry. The complex modulus magnitude ($|G^*| = (G')^2 + (G'')^2$), which reflects material stiffness, remains consistent with deformation up to 6 % strain for both ALG and ALG-B (Fig. S2-a). To ensure linear viscoelastic behavior, a strain of 1 % was selected for subsequent experiments. Figs. S2-b and c show the shear storage and loss moduli's variation with frequency for both compositions, showing an increase as frequency rises. These findings suggest that the B loaded in the hydrogels could form calcium borate particles that will disperse uniformly within the hydrogel, acting as a reinforcement (Fig. S2-a and b), as evidenced by the elevated values of $|G^*|$ and G' observed in ALG-B hydrogels compared to the lower G" values obtained in ALG.

Fig. S3 presents a cytotoxicity assay of ALG and ALG-B hydrogels in direct contact with differentiated C2C12 muscle cells. Both materials showed good biocompatibility with no cytotoxic effects.

Four subcutaneous injections in the quadriceps of 100 μL of either saline solution (ALS), ALG hydrogel (ALS ALG), or ALG B-loaded (ALS ALG—B), were administered to $SOD1^{G93A}$ mice, starting before visible symptoms onset (68 days old) and continuing every two weeks (82, 96 and 110 days old). Treated mice, male and female, were organized in two parallel experiments: i) Symptomatic mice: three groups ($n = 6$), ALS control, ALS ALG, and ALS ALG—B, sacrificed at 115 days old for muscle and nerve evaluation independently of their clinical stage. ii) Symptomatic mice for survival (SV) assessment: two groups ($n = 10$), ALS SV control and ALS ALG-B SV, sacrificed at their final endpoint (ranging between 120 and 146 days). Changes in body weight and motor impairment were tracked over 12 weeks. One of the key features of ALS in the $SOD1^{G93A}$ mouse model is the development of severe muscle atrophy, resulting in progressive weight loss and a marked decline in muscle strength. [29] As shown in Fig. 1-a, mice treated with ALG-B maintained higher body weight over time and achieved the best performance in the four-limb hanging test (Fig. 1-b) indicating preserved motor function compared to untreated controls.

Mutant $SOD1^{G93A}$ mice with elevated copy numbers generally maintain good health until around 80–90 days of age, even though at 60 days old they show altered muscle electromyography indicating muscle denervation. After 80–90 days old, they manifest visible symptoms of motor neuron disease, including limb tremors during suspension. By 120 days, most of these mice progress to advanced disease stages, resulting in complete paralysis. [29] In addition to motor impairment, we monitored visible symptom progression in the survival (SV) experimental group. Supplementary Table 1 illustrates the onset, endpoint, and duration of symptoms in each group. The group treated with ALG-B exhibited a delayed onset of symptoms and an extended survival period (Fig. 1c), although these differences did not reach statistical significance according to the Log-rank (Mantel–Cox) test. However, despite the lack of statistical significance, we consider this trend to be biologically relevant. It is consistent with other statistically significant findings, including improved motor behavior (Fig. 1-a,b) suggesting an overall therapeutic benefit. Given the multifactorial and heterogeneous nature of ALS progression, small extensions in survival, particularly when supported by converging functional and histological improvements, may still reflect a meaningful treatment effect.

The observed improvement in motor function, delayed symptom onset, and extended survival following local muscle treatment, suggest the active role of muscle tissue in ALS pathology, beyond motor neuron degeneration.

a, b) Changes over time in weight and hanging time of mice (male and female) distributed in the different groups. Mice were subcutaneously injected with 100 μL of saline solution (ALS), ALG hydrogel (ALS ALG), or ALG B-loaded (ALS ALG—B) at 68, 82, 96 and 110 days old. Note that all the mice participating in the two parallel experiments, symptomatic mice, and terminal-stage mice for evaluation of survival (SV) were used for the measurements (ALS, $n = 16$; ALG, $n = 6$, ALG—B, $n = 16$). To accomplish with the 3 R's principle, the ALG group ($n = 6$) was not duplicated in the SV experiment since the derived results from this group are equivalent to those obtained from ALS control group. Statistics are shown as mean ± standard deviation. Data were analyzed by an ordinary one-way ANOVA test and corrected for multiple comparisons using Tukey's correction analysis ($p = 0.05$). Statistics indicate differences between groups compared to ALS control group. $^{****}p < 0.0001$, $^{**}p < 0.01$, $^{*}p < 0.05$.

c) Kaplan-Meier survival curves of ALS ($n = 10$) and ALS ALG-B ($n =$

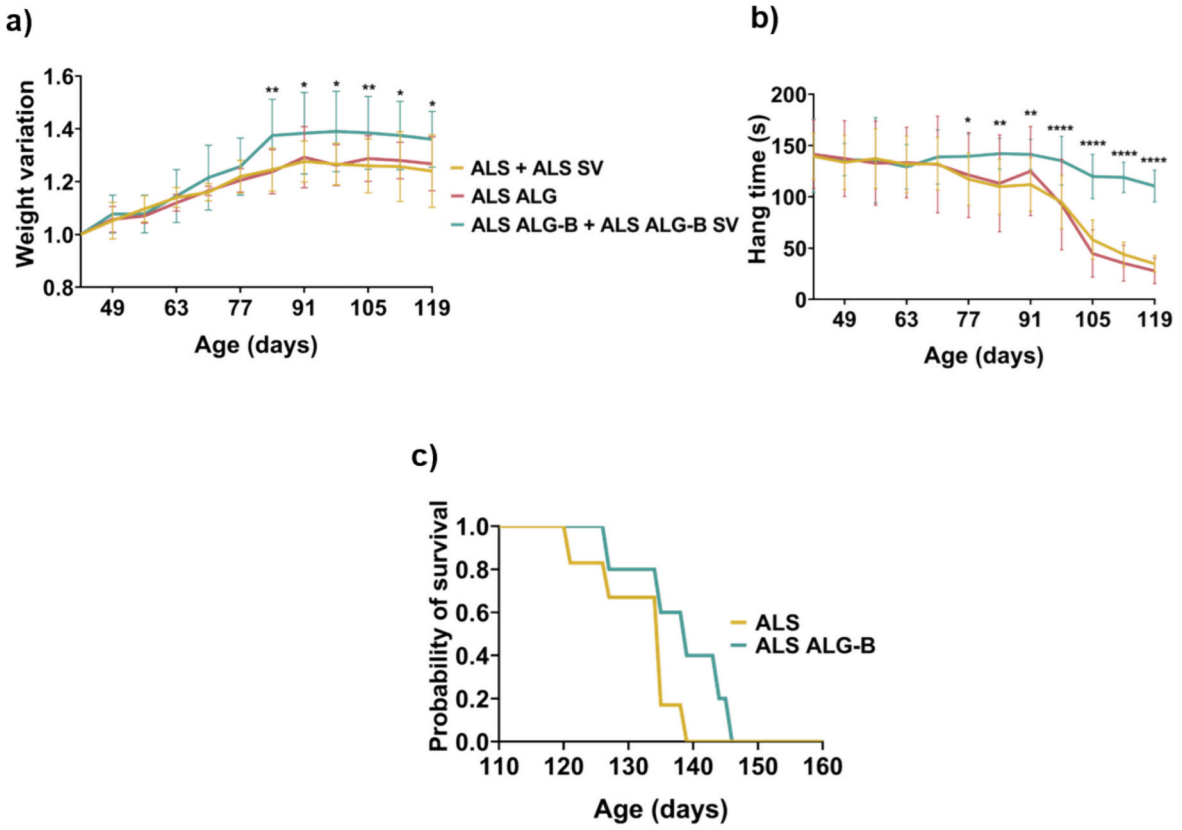

Fig. 1. Evaluation of behavioral motor impairment and analysis of survival.

10) mice. Comparisons of survival curves were evaluated by Log-rank (Mantel-Cox) test. Note that to accomplish with the 3 R's principle, the ALG group was not duplicated in the SV experiment since the derived results from this group are equivalent to those obtained from ALS control group.

2.2. Local B-release counteracts muscle atrophy in symptomatic and terminal-stage SOD1^{G93A} mice

After euthanasia, muscle tissues were histologically analyzed, revealing typical features of denervation-induced atrophy, including angular atrophic fibers, compensatory hypertrophy, variability in fiber size, reduced diameter, and increased nuclear clumps between myofibers. [30,31] Fig. 2 shows quadriceps histoarchitecture in symptomatic (Fig. 2a) and terminal-stage (Fig. 2b) mice, while Fig. S4 depicts the segmentation method used for full tissue quantification.

In both animal experiments, the ALS and ALG control groups exhibited reduced muscle fiber size, presence of atrophic fibers adjacent to hypertrophic ones, and increased nuclear density, features consistent with muscle atrophy, a known hallmark of ALS (Fig. 2, arrows). Thickening of the perimysium and endomysium, likely due to extracellular matrix accumulation, was also observed, suggesting early fibrotic changes.

Although pathological alterations remained present in treated animals, ALG-B treated-mice showed a significant increase in muscle fiber diameter. This suggests a partial attenuation of atrophy progression, in line with the improved motor function observed in the hanging test (Fig. 1). Additionally, treated mice displayed reduced fiber size variability, reflected by a lower coefficient of variance (VC), and a higher proportion of larger-diameter fibers. These findings may reflect enhanced regenerative activity or stabilization of muscle architecture in response to the treatment.

The observation of reduced muscle atrophy in both symptomatic and terminal-stage mice suggests a lasting impact of B treatment over time. Remarkably, just four injections of the treatment were sufficient to decelerate muscle atrophy progression, and these effects persisted until the end of the animals' lives (ALG-B SV, Fig. 2-b), even though the animals still exhibited ALS pathology and ultimately succumbed to the disease, likely due to the extensive neurological damage.

Histoarchitecture of symptomatic ($n = 6$) (a) and terminal-stage (SV) ($n = 10$) (b) muscle quadriceps visualized by hematoxylin/eosin staining. In both animal experiments, the ALG-B group displayed reduced muscle atrophy, as evidenced by a decrease in atrophic fibers (10–20 μm, black arrows) surrounded by hypertrophic fibers (50–60 μm, yellow arrows). Scale bar 50 μm.

Image analysis quantification of morphometric parameters including minimal Feret's diameter and variability among fibers (Variance coefficient, VC). The ALG-B group exhibited a significant increase in the minimal Feret's diameter and a decrease in VC, indicating a more uniform distribution of fiber sizes and the highest number of fibers with increased minimal Feret's diameters. $n > 25{,}000$ fibers per group.

Statistics are shown as mean ± standard deviation. For comparison between the three groups (ALS, ALG and ALG—B), data were analyzed by an ordinary two-way ANOVA test and corrected for multiple comparisons using Tukey's correction analysis ($p = 0.05$). For comparisons between the two groups (ALS SV, ALG-B SV), data were analyzed by an unpaired *t*-test applying Welch's corrections ($p = 0.05$). ****$p < 0.0001$.

2.3. Local B-release preserves fast (type II) muscle fibers, augments satellite Pax7^{+} cells and reduces SOD1 and fibronectin expression in symptomatic and terminal-stage skeletal muscle of SOD1^{G93A} mice

Skeletal muscle is characterized by a heterogeneous composition of two types of fibers. Type I (slow-twitch) fibers, optimized for endurance activities, have a high content of myoglobin, essential for providing instant oxygen, and abundant mitochondria. Type II (fast-twitch) fibers

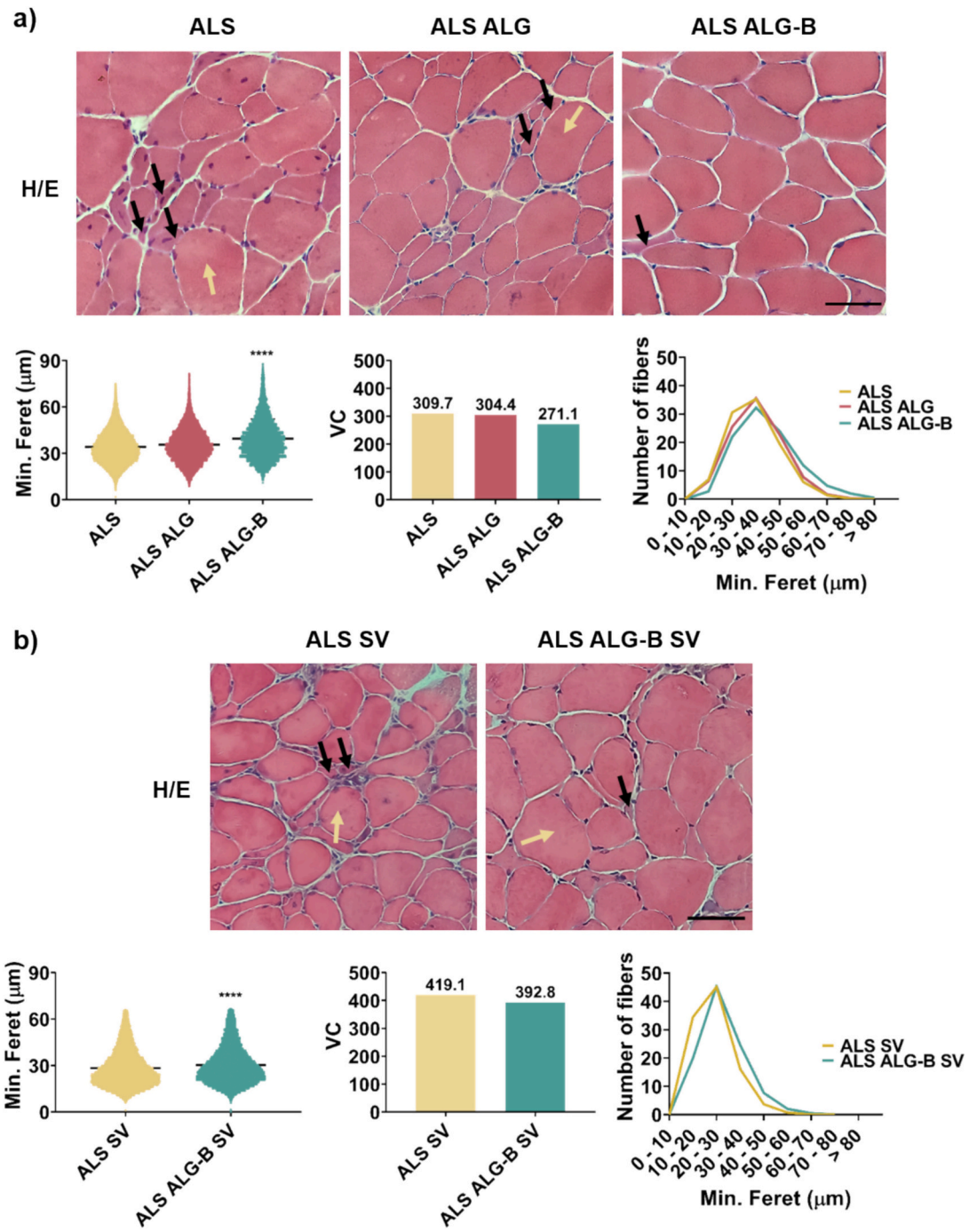

Fig. 2. Morphometric muscle parameters in symptomatic and terminal-stage mice.

are designed for short bursts of intense activity, have a major number of neuromuscular junctions, and contain large amounts of glycogen as a source for anaerobic glycolysis. [32]

In ALS, muscle denervation is accompanied by a progressive replacement of type II by type I fibers. This phenomenon, reported in both murine models and patients, highlights the vulnerability of fast-twitch fibers, which predominantly exhibit an atrophic appearance, while slow-twitch fibers adopt a compensatory hypertrophic morphology. [30,31]

An immunofluorescence analysis result of various muscle markers relevant to ALS is shown in Fig. 3. Following B treatment, we observed a substantial decrease in type I slow myofibers in the ALG-B muscle of both symptomatic and terminal-stage mice. Our findings suggest a potential preservation of type II fast myofibers. Given that type II fast fibers are the initial targets of atrophy in ALS, our results imply that the treatment is inhibiting the pathological myofiber transition characteristic of ALS. This aligns with our previous histological observations indicating a mitigation of muscle atrophy (Fig. 2).

Several lines of evidence highlight the impact of ALS on muscle turnover, revealing that impaired myogenic processes could aggravate denervation-induced muscle wasting. Muscle denervation re-innervation cycles occurring in ALS, are accompanied by satellite cells activation ($Pax7^{+}$ cells) that play an essential role in the intrinsic repairing mechanisms of muscle. ALS skeletal muscle satellite cells present impaired activity and myogenic potential. In ALS patients, Pax7 expression decreases [31] and satellite cells become activated but do not

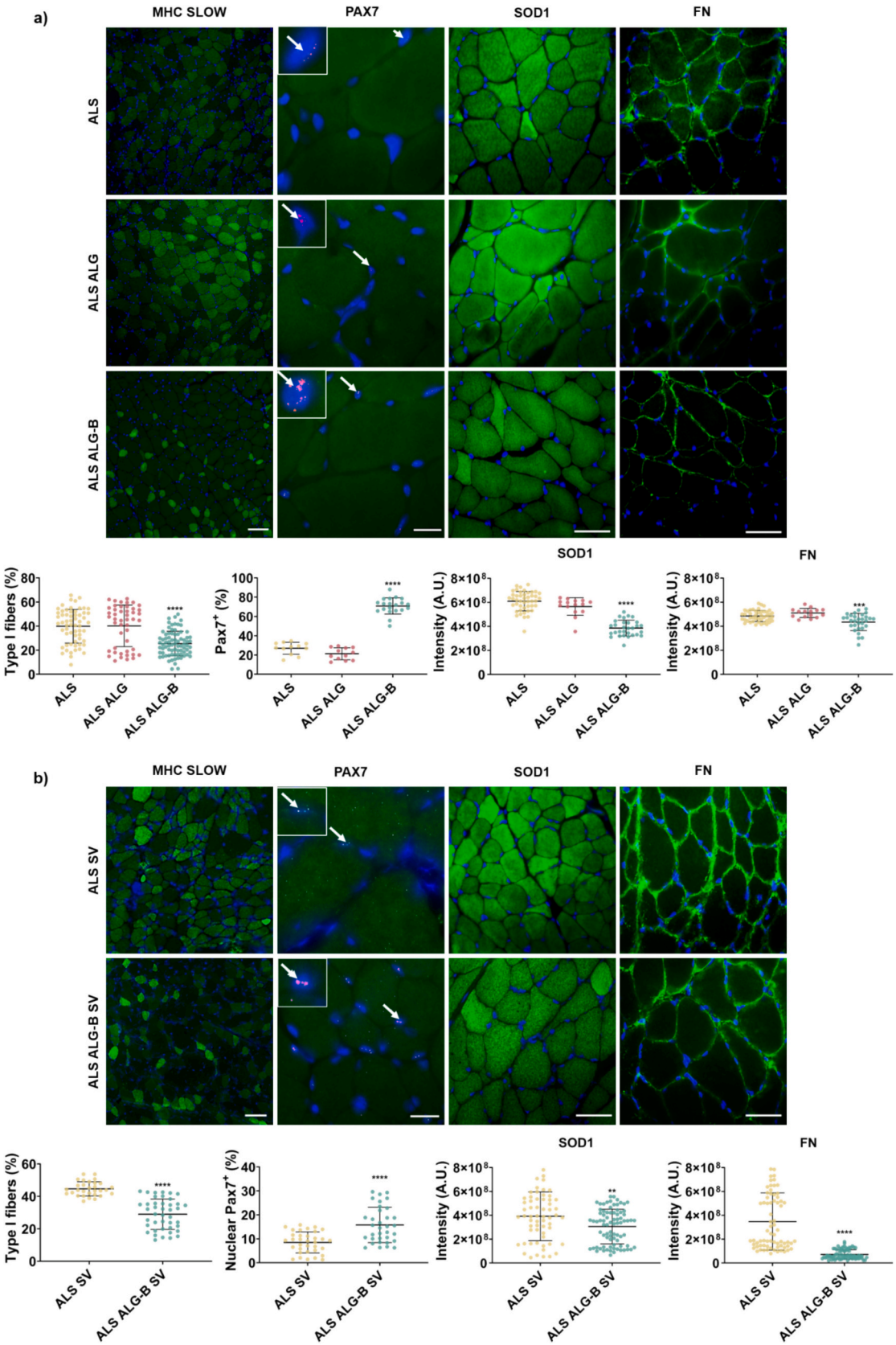

Fig. 3. Immunofluorescence detection of ALS muscle markers in symptomatic and terminal-stage mice.

progress through the myogenic program exhibiting incomplete differentiation and abnormal myotube and senescent-like morphology. [33–35] In the SOD1^{G93A} mouse model, satellite cells exhibit compromised cell proliferation capacity, even during the pre-symptomatic disease stages along with a reduction in the number of Pax7^{+} cells. [36,37]

Fig. 3-a,b shows a significant increase in Pax7^{+} cells in ALG-B–treated mice compared to controls, in both symptomatic and terminal stages. The higher percentage of Pax7^{+} cells in symptomatic *versus* terminal-stage ALS controls, reflects the natural progression of the disease and aligns with previous reports of a decline in satellite cell populations over time. [36,37] Given the reduced number and compromised proliferation of satellite cells in the SOD1^{G93A} model, our results indicating a substantial rise in active satellite cells suggest that B is potentiating and enhancing muscle regeneration and repair processes. Together with the observed improvements in muscle strength and overall motor function (Fig. 1), it suggests that satellite cells are not only active, but they are also effectively progressing through the myogenic program reflecting an enhanced capacity for muscle healing. Furthermore, the observed increase in Pax7^{+} cells found also in terminal-stage mice, who were in the advanced stages of the disease, indicates that treatment is offering long-term improvement potentially slowing down the progression of muscle degeneration.

We have also evaluated superoxide dismutase 1 (SOD1) and fibronectin (FN) protein expression (Fig. 3-a,b). SOD1 is a critical player in the anti-oxidative defense. The SOD1^{G93A} mouse model employed, carries several copies of the human SOD1G93A mutation (glycine to alanine at position 93) which results in a ubiquitous toxic gain of SOD1 function. [38,39] Specifically, skeletal muscle has been described as a primary target of SOD1^{G93A}-mediated toxicity on which oxidative stress triggers muscle atrophy. [40]

ALG-B-treated symptomatic and terminal-stage mice presented a reduction in total SOD1 protein expression indicating that treatment is helping to protect muscle from toxic SOD1 oxidative stress effects slowing down muscle deterioration, and conferring an improved muscle function and strength, which translates into enhanced motor function observed in Fig. 1 and reduction in muscle atrophy (Fig. 2). Further investigation is needed to decipher the specific mechanism by which B reduces SOD1 protein expression, even though our results suggest that ALG-B treatment is specifically targeting SOD1 within the muscle and could represent a promising therapeutic approach.

In addition, after muscle denervation processes, augmented FN protein expression have been reported in both ALS patients [41] and SOD1^{G93A} mice, [42] related to the appearance of fibrotic changes. An active fibrotic process has been reported in the skeletal muscle of symptomatic SOD1^{G93A} mice. [42]

FN levels were also diminished in symptomatic and terminal-stage mice after treatment concordant with the observation of a reduced thickness of perimysium and endomysium (Fig. 3-a,b), suggesting a reduction in muscle fibrosis levels related to FN overexpression.

Overall, our findings at the protein expression in muscle histopathology, align with the observed recoveries in motor function (Fig. 1) and the deceleration of muscle atrophy progression (Fig. 2) indicating that local B treatment is exerting a positive impact on muscle integrity and function.

Immunofluorescence detection of slow type I fibers, Pax7^{+} satellite cells, SOD1 and FN protein expression. Quadriceps sections of symptomatic ($n = 6$) (a) and terminal-stage ($n = 10$) (b) mice were analyzed. In both animal experiments, the ALG-B group displayed reduced slow type I fibers, SOD1 and FN protein expression, in line with the observation of a reduction of muscle atrophy after the treatment and with the increase in Pax7^{+} cells. Scale bar 50 μm. Graphs represent the image analysis quantification of the intensity of the different markers. $n > 12$ images per mouse.

Statistics are shown as mean ± standard deviation. For comparison between the three groups (ALS, ALG and ALG—B), data were analyzed by an ordinary two-way ANOVA test and corrected for multiple comparisons using Tukey's correction analysis ($p = 0.05$). For comparisons between the two groups (ALS SV, ALG-B SV), data were analyzed by an unpaired *t*-test applying Welch's corrections ($p = 0.05$). $^{****}p < 0.0001$, $^{***}p < 0.001$, $^{**}p < 0.01$.

2.4. Evaluation of muscle inflammation indicates that muscle B-release reduces mast cell inflammatory response in symptomatic and terminal-stage SOD1^{G93A} mice

In ALS, inflammation is a key mechanism contributing to the degeneration process of both motor neurons and muscles. Several reports describe the presence of inflammatory cells within peripheral nerves and skeletal muscles of ALS patients and rodents. [43,44] Among inflammatory cells, the granulated hematopoietic-derived mast cells, activate upon tissue damage and orchestrate the inflammatory responses recruiting and activating other immune cells through degranulation and release of inflammatory mediators and enzymes, [45–48] mediating neurogenic inflammation. [49] Recent findings suggest that mast cells directly interact with degenerating motor nerve endings and motor endplates in the skeletal muscle of SOD1^{G93A} rodents with their number and degranulation pattern correlating with the progression of paralysis, [44] highlighting their involvement in the chronic inflammatory muscle response in ALS. [50,51]

Fig. 4-a shows representative images of nerve, blood vessel structures and mast cells. The assessment of muscle mast cell recruitment revealed that in symptomatic mice (Fig. 4-b), there was an elevation in the total number of infiltrated mast cells in the control groups (ALS, ALG), along with an increase in degranulated mast cell count and mast cell proximity to nerves. However, the ALG-B treated group showed a significant reduction in the density of infiltrated mast cells as well as the degranulating mast cell number, suggesting an inhibition of mast cell migration and activation. Further, in B-treated quadriceps mast cells were mainly perivascular located and not near nerve fibers, suggesting that B may downregulate mast cell-mediated inflammatory events influencing the degeneration of the muscle and the peripheral motor pathway.

In terminal-stage mice (Fig. 4-c), we found high levels of total and degranulated mast cells, even in treated ALS ALG-B mice, indicating an ongoing pro-inflammatory process consistent with the disease's advanced progression. Consequently, in terminal-stage mice, the total number of mast cells surrounding nerve fibers in control groups were higher compared to symptomatic control mice, reflecting the extensive nerve inflammation characteristic of the SOD1 mouse model (Fig. 4-b,c). Nevertheless, despite the pronounced inflammation present in the terminal-stage ALS muscle, ALG-B treated mice exhibited a significant reduction in mast cells in the nerve periphery. This suggests that while inflammation persists at a later stage, the treatment appears to delay its onset.

(a) Representation of nerve, blood vessel structures and mast cells indicated by yellow, red and black arrows respectively.

Analysis of mast cell recruitment in muscle by toluidine-blue B staining. Quadriceps sections of symptomatic ($n = 6$) (b) and terminal-stage ($n = 10$) (c) mice were analyzed. Nerves are indicated by yellow arrows.

In symptomatic mice, the ALG-B group presented a strong decrease in the density of infiltrated mast cells as well as the de-granulating mast cell number. Further, mast cells were mainly perivascular located and not close to a nerve fiber, a hallmark characteristic of extensive nerve inflammation occurring in SOD1^{G93A} mice. In terminal-stage mice, the ALG-B group presented a strong decrease in mast cells in the nerve periphery, suggesting a delay in the inflammation onset despite the active inflammation process.

Scale bar: 50 μm. Graphs represent the image analysis quantification of the percentage of mast cells in each location, the total number of mast cells, and the total number of de-granulated mast cells. $n > 40$ images

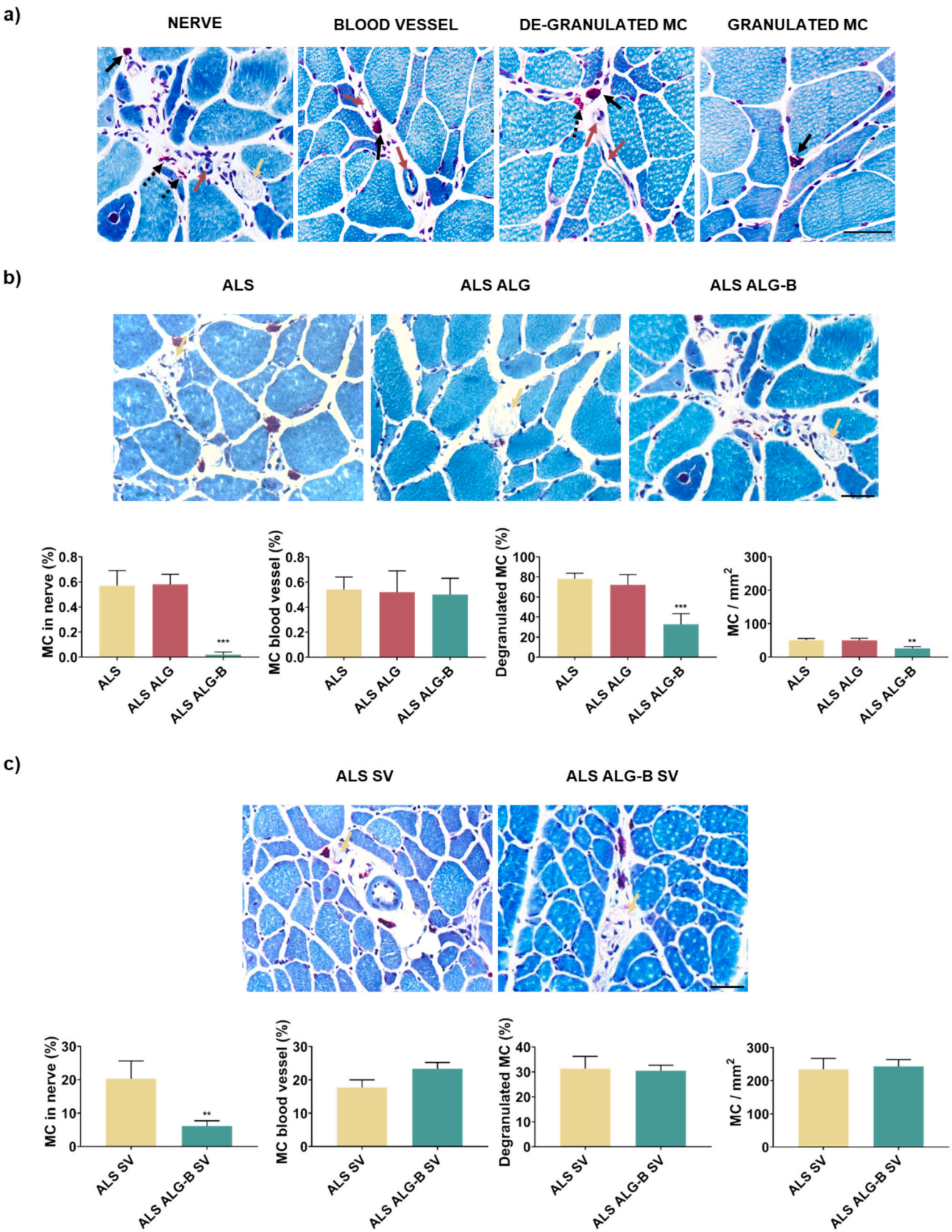

Fig. 4. Infiltration and degranulation of mast cells into the skeletal muscle of symptomatic and terminal-stage SOD1^{G93A} mice.

per group.

Statistics are shown as mean ± standard deviation. For comparison between the 3 groups (ALS, ALG, ALG—B), data were analyzed by an ordinary one-way ANOVA test and corrected for multiple comparisons using Tukey's correction analysis ($p = 0.05$). For comparisons between 2 groups (ALS SV, ALG-B SV), data were analyzed by an unpaired *t*-test applying Welch's corrections (p = 0.05). ***$p < 0.001$. **$p < 0.01$.

We have further analyzed IL-6 muscle levels, a cytokine known for its diverse functions and crucial role in immune response, inflammation, metabolism, and hematopoiesis. When the production of IL-6 becomes dysregulated, it can lead to the development of various chronic inflammatory diseases. [52] This cytokine is produced by immune and blood cells, endothelial cells, and myocytes during muscle contraction. [53] Interestingly, elevated levels of IL-6 have been observed in ALS patients, which is associated with motor neuron degeneration. [54] Additionally, IL-6 has been found to contribute to muscle atrophy after denervation, further highlighting the involvement of cytokines in the progression of ALS. Given its significance, IL-6 has emerged as a potential biomarker for ALS and a target for therapeutic interventions, as demonstrated by ongoing clinical trials. [55]

Fig. S5 illustrates the immunofluorescence detection and image analysis quantification of IL-6 in symptomatic and terminal-stage mice. In both experiments, the control mice exhibited elevated levels of IL-6. Notably, the IL-6 levels were significantly higher in terminal-stage control mice, consistent with previous findings that associate IL-6 with disease progression. [55] However, the quadriceps muscles treated with B (ALG—B) presented reduced IL-6 levels, indicating a decrease in the inflammatory response within the muscle tissue following treatment. These findings collectively suggest that B may function as a therapeutic agent by promoting muscle repair processes, suppressing mast cell-mediated inflammatory events, reducing pro-inflammatory cytokines such as IL-6, and mitigating muscle degeneration and neuroinflammation.

To further explore the inflammatory environment in ALS muscle and its modulation by the treatment, we evaluated the expression of Transforming Growth Factor- β (TGF-β), a cytokine known to be involved in both fibrosis and muscle differentiation. As shown in Fig. S6, immunofluorescence analysis revealed that TGF-β levels were significantly reduced in the muscle tissue of ALG-B–treated mice compared to ALS and ALG controls, in both the symptomatic and terminal-stage mice. This reduction in TGF-β, together with previously observed decreases in IL-6, suggests that the treatment contributes to a less inflammatory and more pro-regenerative microenvironment, which may support the observed improvements in muscle architecture and function.

2.5. Local muscle B-release induces motor neuron preservation and reduces glial inflammation in the spinal cord in symptomatic and terminal-stage SOD1^{G93A} mice

Following the assessment of muscle inflammation, which revealed diminished inflammation specifically near muscle nerve fibers (Fig. 4, S5, S6), and the observed changes in improved motor behavior (Fig. 1) and improved muscle health (Figs. 2, 3) that indirectly can potentially be associated with enhanced motor function or survival, we aimed to determine if the administration of a localized muscle treatment to ALS SOD1^{G93A} mice could lead to neuroprotection. To do that we ensured comprehensive measurement coverage of the mouse spinal cord by employing a meticulous dissection protocol that encompassed the entirety of the spinal column. We analyzed each spinal cord segment, spanning from the cervical to the sacral region, encompassing all corresponding vertebral levels (cervical, thoracic, lumbar and sacral) of symptomatic and terminal-stage SOD1^{G93A} mice.

The SOD1^{G93A} model is characterized by motor neuron degeneration caused by the toxic effects of the SOD1 mutant protein, which affects both motor neurons and their neighboring glia. [38,56] In Fig. 5, we show a representative image of spinal cord and detail of motor neuron located in the ventral horn (a). Our findings revealed a notable and significant increase in the number of motor neurons in totality of the spinal cord of both symptomatic (b) and terminal-stage (c) mice following local muscle treatment compared to the control groups. These results suggest that the treatment applied to the muscle tissue may have broader effects on the central nervous system in ALS, potentially influencing the neurodegenerative process and preserving motor neurons beyond the targeted muscle area. Our results are in line with previous studies indicating that preservation of muscle tissue function can slow motor neuron degeneration, [57] despite overexpression of mutant SOD1 in rodents induces inevitably a neuropathic phenotype. Furthermore, we conducted measurements to quantify the white matter area in the totality of the spinal cord (Fig. 5b- and c). Our results indicated that both symptomatic and terminal-stage mice treated with ALG-B exhibited also an increased white matter area, indicating the preservation of neuronal axon integrity. These findings align with the observed reduction in inflammation shown in Figs. 4 and S5 and S6.

To further investigate the neurobiological impact of muscle-directed treatment, we analyzed the expression of Nerve Growth Factor Receptor (NGFR-p75NTR) in the spinal cord. NGFR is a multifunctional receptor involved in both neuronal survival and apoptosis, depending on the cellular context and its interaction with co-receptors and ligands [58]. As shown in Fig. S7, NGFR expression was significantly increased in the ALG-B treated groups compared to ALS controls, in both symptomatic and terminal-stage mice. This upregulation may reflect a compensatory or protective response to muscle regeneration, potentially favoring neuronal plasticity or survival signaling in the spinal cord. These findings support the idea that peripheral muscle repair can influence central nervous system responses, contributing to the broader therapeutic effect of the treatment.

While the beneficial effects observed in treated mice are consistent with NaBC1 activation, based on our previous studies [24–27] and our recent discovery of the new role of NaBC1 in mechanotransduction, [23] it is also possible that B contributes to muscle regeneration and neuroprotection through additional mechanisms, such as modulation of the local inflammatory environment involving parallel pathways that will require future studies.

a) Representative image of spinal cord (lumbar segment) stained with toluidine-blue B (scale bar 250 μm) and detail of motor neuron located in the ventral horn (scale bar 50 μm). Motor neuron count and white matter area in the spinal cord were assessed in symptomatic (b) and terminal-stage (c) mice. The spinal cord was divided into cervical, thoracic, lumbar and sacral segments, and multiple histological sections from each segment were analyzed. The B treatment applied in muscle induced an increase in motor neuron number and white matter area in the spinal cord in both groups. $n \geq 6$ mice per condition.

Statistics are shown as mean ± standard deviation. For comparison between the three groups (ALS, ALG, ALG—B), data were analyzed by an ordinary one-way ANOVA test and corrected for multiple comparisons using Tukey's correction analysis ($p = 0.05$). For comparisons between 2 groups (ALS SV, ALG-B SV), data were analyzed by an unpaired *t*-test applying Welch's corrections (p = 0.05). ****$p < 0.0001$, ***$p < 0.001$, *$p < 0.05$.

In addition to the selective degeneration of motor neurons, astrogliosis is a prominent characteristic of ALS. Astrocytes, a type of glial cell, maintain neuronal homeostasis and provide support and protection for efficient neuronal function. However, in pathological conditions, activated astrocytes can have harmful effects on neuronal survival. Glial fibrillary acidic protein (GFAP) is an intermediate filament protein that is highly expressed in reactive astrocytes and is significantly upregulated in the spinal cord of ALS patients and mouse models, where reactive astrogliosis is prominent. [59] The increased production of GFAP has been linked to modulatory roles in the progression of ALS. [60] In Fig. 6, we examined the detection of GFAP in the complete spinal cord of both symptomatic and terminal-stage SOD1^{G93A} mice. Similar to the observations made regarding mast cells, IL-6 and TGF-β levels in muscle tissue

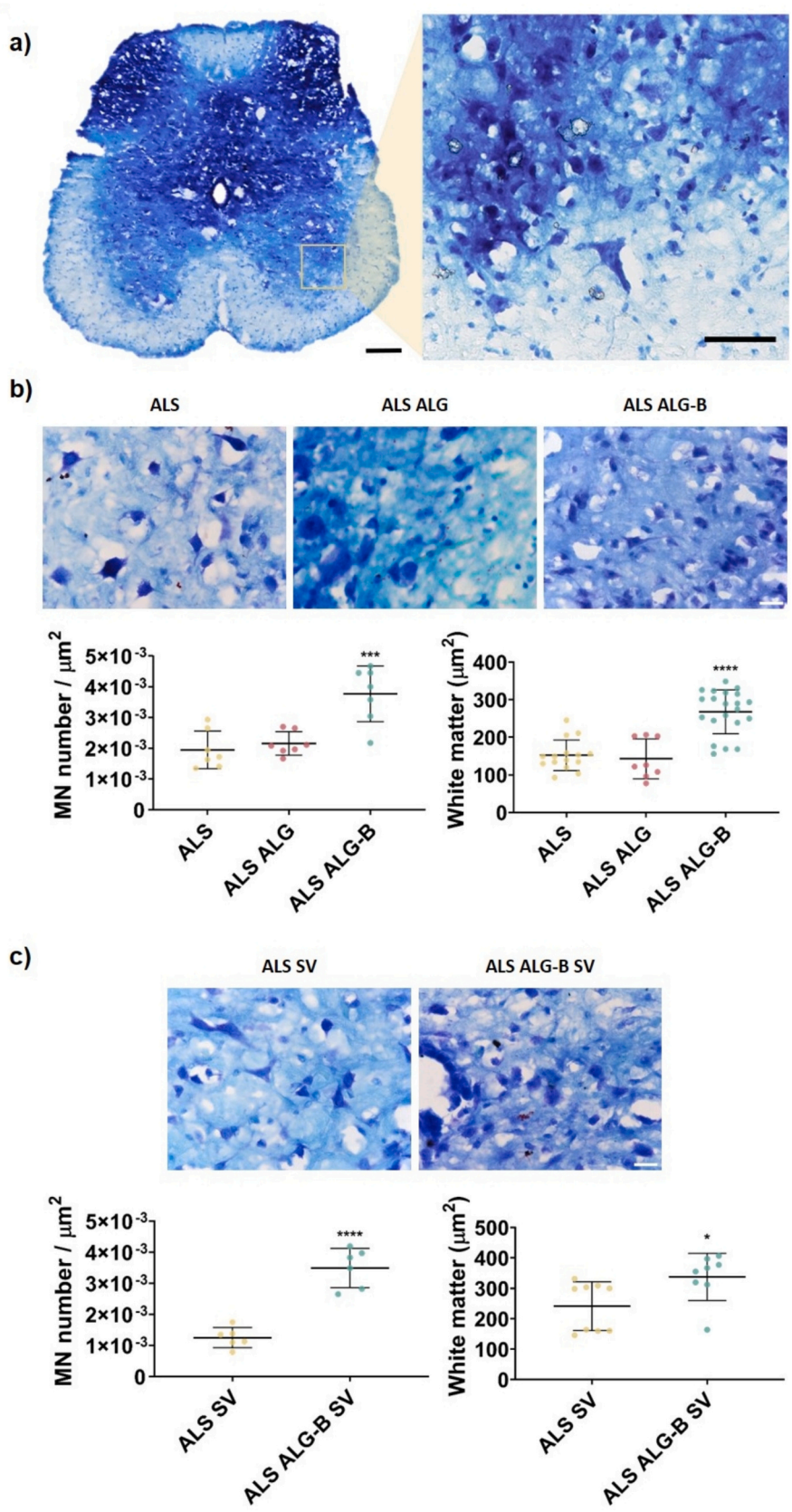

Fig. 5. Evaluation of motor neuron preservation in spinal cord in symptomatic and terminal-stage SOD1^{G93A} mice.

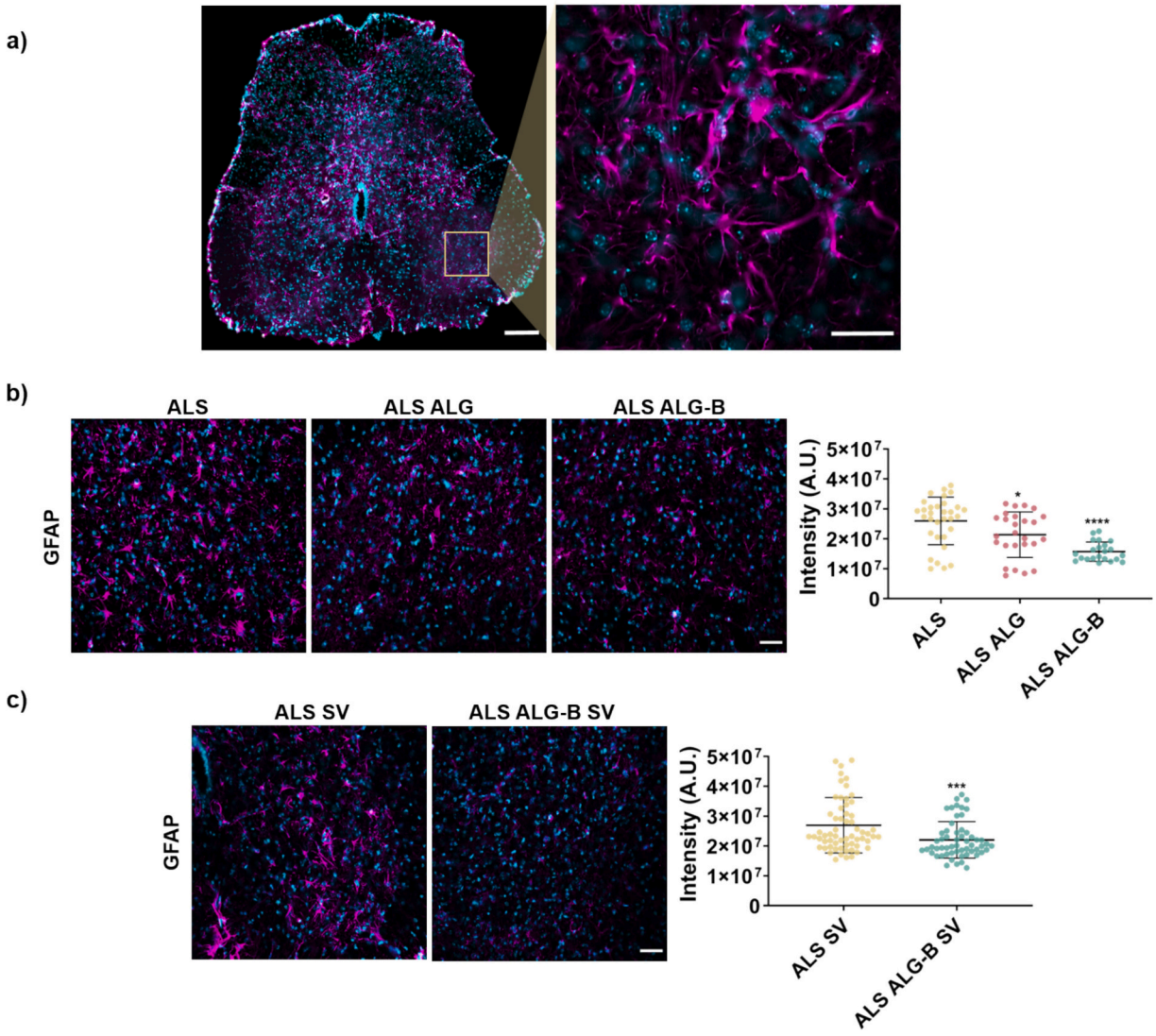

Fig. 6. Evaluation of glial-mediated inflammation in the spinal cord in symptomatic and terminal-stage SOD1^{G93A} mice.

(Figs. 4, S5, S6), we found that neuro-inflammatory levels were significantly higher in terminal-stage mice, corroborating that the GFAP protein gradually increases with disease progression, consistent with previous reports. [57] Interestingly, following the local muscle treatment, we observed a reduction in GFAP values in the treated mice from both experiments. These findings indicate that the application of B in muscle has the potential to modulate neuro-inflammation processes that take place in ALS. However, it is important to note the possibility of a direct impact of B on glial cells and motor neurons. Additional research is necessary to unravel the precise cellular-level function of B and NaBC1 in the nervous system.

a) Representative image of the spinal cord (lumbar segment) (scale bar 250 μm), with detailed ventral horn area where astrocytes are detected with GFAP antibody (magenta, scale bar: 25 μm). Cellular nuclei were detected with DAPI.

Immunofluorescent detection and quantification of GFAP in symptomatic ($n = 6$) (b) and terminal-stage ($n = 10$) (c) mice. Scale bar 50 μm. ALG-B treatment decreases GFAP expression, indicating a reduction of neuro-inflammation. $n > 30$ images per group.

Statistics are shown as mean ± standard deviation. For comparison between the three groups (ALS, ALG, ALG—B), data were analyzed by an ordinary one-way ANOVA test and corrected for multiple comparisons using Tukey's correction analysis ($p = 0.05$). For comparisons between the two groups (ALS SV, ALG-B SV), data were analyzed by an unpaired *t*-test applying Welch's corrections (p = 0.05). ****$p < 0.0001$, ***$p < 0.001$, *$p < 0.05$.

2.6. Analysis of muscle gene expression in symptomatic and terminal-stage SOD1^{G93A} mice

After the euthanasia of symptomatic and terminal-stage mice, quadriceps muscles were used for RNA extraction and analysis of gene expression (Fig. 7).

In our previous works, we have shown *in vitro* that NaBC1 co-localizes with FN-binding integrins ($\alpha_5\beta_1$ and $\alpha_v\beta_3$) after activation, and cooperates with GFR stimulating intracellular signaling. [24–26]

The skeletal muscle extracellular matrix (ECM) is a dynamic structure primarily comprised of laminins (LM), collagens, proteoglycans, and FN. This intricate network plays a pivotal role in regulating the physiological functions of muscles. [61,62] Specifically, FN holds a crucial position in muscle regeneration by aiding in the proliferation and differentiation of satellite cells. [63] Moreover, FN-binding integrins such as $\alpha_5\beta_1$ and $\alpha_v\beta_3$ contribute significantly to muscle stability and exert a regulatory influence on the repair processes. [64,65] Within the skeletal muscle tissue, integrins form connections with the ECM, facilitating interactions among muscle cells within their environment. These

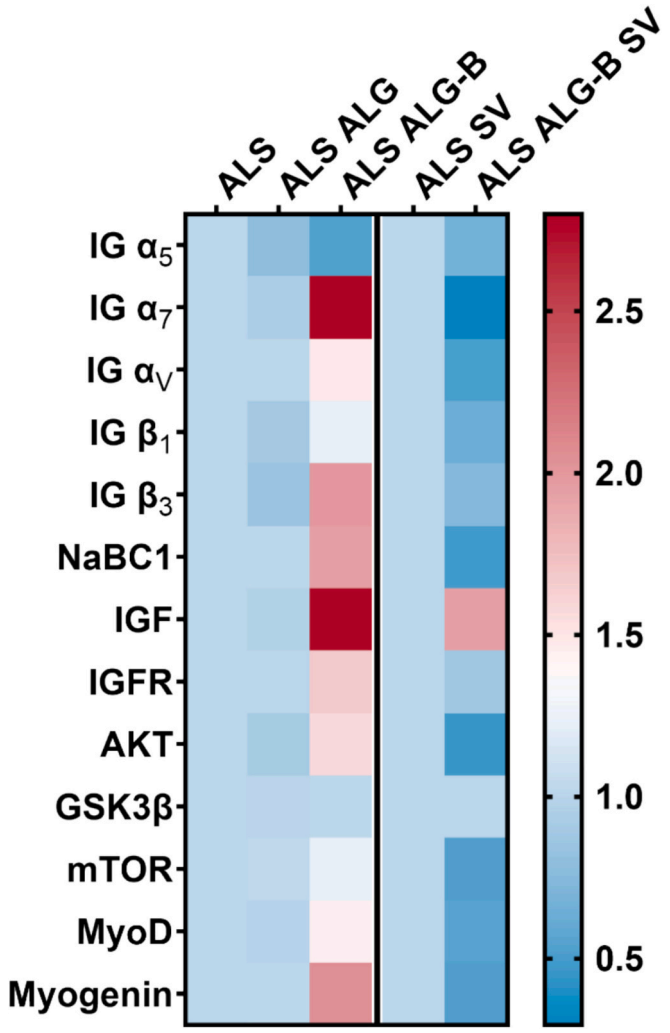

Fig. 7. Representative heat map analysis of the up/down-regulated genes in the muscle of symptomatic and terminal-stage SOD1^{G93A} mice.

interactions are vital for muscle cell adhesion, migration, and differentiation. [66]

In this work, aiming to confirm the interplay between NaBC1 and integrins for muscle recovery *in vivo*, we have evaluated FN-binding ($\alpha_5\beta_1$ and $\alpha_v\beta_3$) and LM-binding ($\alpha_7\beta_1$) integrins expression. $\alpha_7\beta_1$ integrin, is specifically associated with skeletal muscle playing a key role in muscle stability, function, and repair [67] and acts as a critical mechanosensor contributing to mechanical-load induced skeletal muscle growth. [68]

Our results showed that symptomatic mice treated with ALG-B hydrogels presented a markedly upregulated mRNA expression of α_7, α_v, β_1 and β_3 integrins, ranging from a 1.2 to 2.8-fold rise (Fig. 7), in comparison to the controls. This indicates a stimulation of muscle repair and regeneration after muscle local treatment. Particularly noteworthy was the substantial 2.8-fold increase in mRNA expression of α_7 integrin. Given the pivotal role played by $\alpha_7\beta_1$ integrin in skeletal muscle ECM attachment and muscle force development [69], the absence of this integrin causes muscle defects and myopathy. [70] Moreover, elevating α_7 levels has been employed as a strategy to counterbalance deficiencies in ECM and cytoskeleton linkage occurring in certain muscular dystrophies, leading to a reduction in muscle pathology. [71] Thus, our results showing induced upregulation of integrin expression, and specifically α_7, after NaBC1 activation, reinforce our hypothesis that considers NaBC1 and integrin stimulation for enhancing the intracellular signaling as we previously reported. [24–26]

Interestingly, despite our previous observations of upregulated α_5 integrin expression *in vitro* during cell adhesion stages following NaBC1 activation in healthy murine muscle cells, [23,26] our current findings show decreased levels of this integrin *in vivo* in symptomatic SOD1^{G93A} mice. Specifically in ALS, α_5 integrin has been shown to be upregulated in the spinal cord and peripheral nerves, contributing to immune cell recruitment and inflammation, factors linked to disease progression. [72] In fact, α_5 has been proposed as a potential therapeutic target since α_5 blocking resulted in improved motor function, delayed disease progression, and increased survival in ALS animal models. [72] Fig. 7 shows that treatment with B-loaded hydrogels halved the expression levels of α_5 integrin in symptomatic mice. Taken together the obtained results describing a reduction of inflammation in spinal cord (Fig. 6) and muscle (Figs. 4, S5, S6), we underscore the potential of B as a therapeutic approach for the treatment of ALS.

We have also observed that mRNA expression of NaBC1 transporter was upregulated in ALG-B symptomatic mice, suggesting a concentration-dependent regulatory mechanism exerted by B in myotubes for NaBC1 expression. To date, no data is available regarding NaBC1 expression regulation in mammalian cells.

Additionally, we evaluated the expression of key genes involved in metabolic pathways known to influence muscle homeostasis and function. Insulin-like growth factor (IGF) promotes myogenesis, proteostasis, and cell growth through the Protein Kinase B (Akt)/ Mechanistic Target of Rapamycin (mTOR) (Akt/mTOR) signaling pathway, which regulates diverse cellular functions including growth, proliferation, and metabolism. [73,74] In our study, symptomatic mice treated with ALG-B hydrogels exhibited a significant upregulation of IGF, IGF receptor (IGFR), Akt, and mTOR mRNA levels compared to controls. While a reduction in Glycogen Synthase Kinase-3 (GSK3β) expression was also observed, this change did not reach statistical significance. Given that GSK3β is known to oppose Akt activity metabolically and has been implicated in ALS pathogenesis through its hyperactivity in non-neural cells, [75] the observed trend remains of interest. Although these findings suggest a potential involvement of the IGF-Akt-mTOR signaling axis in mediating the effects of ALG-B treatment, we acknowledge that further validation at the protein and functional levels is necessary to confirm the activation and role of this pathway. From a therapeutic perspective, considering that IGF has been used as a muscle neurotrophic factor to counteract impairment of the proteostasis observed in ALS [76] our data support the hypothesis that NaBC1 activation may contribute to improved muscle physiology, at least in part, through the modulation of this signaling network.

We have further evaluated two members of the Myogenic Regulatory Factor (MRF) family of transcription factors, Myogenic Differentiation 1 (MyoD) and Myogenin. MyoD is a master gene for myogenesis. Activated satellite cells expressed MyoD at early stages of myogenic differentiation and is crucial for efficient activation and proliferation. [76,77] After MyoD activation in turn induces expression of other myogenic-related genes such as Myogenin. Myogenin participates in myocyte fusion and is essential for regulation of adult myofiber growth and satellite cell homeostasis. [78] Our results further corroborated the B restorative effects in muscles of symptomatic mice showing upregulation of MyoD and Myogenin (1.5 and 2.1-fold increase respectively), and are in line with the observations confirming improvement of motor function (Fig. 1) and muscle atrophy recovery (Fig. 2). However, the results obtained in terminal-stage mice presented a contrasting outcome, displaying a general downregulation of all evaluated genes (Fig. 7 and S8). We attribute this outcome to the severe damage evident in the muscles of these mice, stemming from the extensive muscle denervation process occurring in ALS during the disease's advanced stages. These terminal-stage mice were sacrificed after reaching total paralysis, rendering them unable to self-feed or drink. Despite displaying noticeable improvements in muscle histoarchitecture, particularly in muscle atrophy recovery and inflammation reduction, these mice ultimately exhibited minimal muscle metabolic activity, likely due to energy depletion from

starvation and the absence of electrical stimuli resulting from irreparable damage to motor neurons.

Quantitative real-time PCR analysis of relative mRNA expression of α_5, α_7, α_v, β_1 and β_3 integrins, NaBC1 transporter, members of the IGF-1-Akt-mTOR axis involved in muscle growth, and myogenic regulatory factors (MyoD, Myogenin). $n \geq 6$ mice per condition. Diagrams for each individual real-time PCR analysis are represented in Fig. S8.

3. Conclusions

This study presents a novel muscle-targeted approach for amyotrophic lateral sclerosis (ALS) therapy based on the activation of NaBC1 using injectable borax-loaded alginate hydrogels. In a local proof-of-concept study using $SOD1^{G93A}$ mice, this treatment promoted muscle regeneration, reduced inflammation, and improved motor function and survival. These beneficial effects were accompanied by reduced muscle atrophy, decreased slow type I fibers, SOD1 and FN expression, and increased activation of muscle satellite cells. Additionally, gene expression analyses suggested the involvement of trophic factors and myogenic regulators, including IGF and its receptor, integrins, and markers of myogenic progression. Although mRNA data showed trends in upregulation of Akt and mTOR, further studies at the protein level are required to confirm the functional activation of the IGF-Akt-mTOR axis pathway. Interestingly, we observed retrograde neuroprotective effects in the spinal cord, including reduced glial activation and preservation of motor neuron loss and survival, despite the treatment being administered locally to the quadriceps. These findings support the idea that enhancing peripheral muscle health may influence central nervous system outcomes, possibly through systemic or retrograde signaling mechanisms. While the precise contribution of B beyond the injection site remains to be determined, this opens new questions for ongoing investigation. Importantly, this strategy aligns with therapeutic paradigms already used in other neuromuscular disorders, such as Duchenne muscular dystrophy, where hydrogel-based scaffolds are widely applied for local delivery of bioactive compounds. Our results suggest that similar localized interventions may be adapted for ALS, providing a complementary route to traditional motoneuron-focused therapies. Nevertheless, our study was designed as an initial local proof-of-concept, and the systemic distribution, long-term safety, and potential toxicity of B require further investigation. Additional experiments are underway to clarify these aspects, as well as to evaluate the specific effects of NaBC1 activation on neuronal and glial populations. In summary, our findings highlight the therapeutic relevance of skeletal muscle in ALS and support the development of biomaterial-assisted strategies targeting muscle health. This muscle-directed approach may complement existing therapies targeting motor neuron inflammation and help mitigate neuromuscular degeneration in ALS.

4. Experimental section

4.1. Material substrates

4.1.1. Alginate-based hydrogel preparation

Ultrapure sodium alginate (Pronova™ UP LVM, Novamatrix), was dissolved in 1 % D-mannitol aqueous solution (Sigma-Aldrich) at a concentration of 1.5 %. Borax was dissolved in alginate solutions at 0.16 M concentration. Alginate solution was next filtered through a 0.22 μm pore Minisart Syringe Filter (Sartorius). For gelation, 2.7 mL of the alginate solution was mixed with 60 μL of 1.22 M $CaSO_4{\cdot}2H_2O$ (Sigma-Aldrich) through two Luer Lock syringe (BS Syringe) connected with a Fluid Dispensing Connector (Braun). Alginate and $CaSO_4{\cdot}2H_2O$ were mixed 10 times until complete homogenization. To retard the gelation time and produce injectable hydrogels, 60 μL of 0.5 M $Na_2HPO_4{\cdot}2H_2O$ (Panreac) was added to the cross-linking reaction.

4.1.2. B-release determination

The *in vitro* release of B previous to the animal experimentation was performed by immersing the alginate-based hydrogel (ALG and ALG—B), prepared with Na_2HPO_4 at 0.5 M, in 1 mL of DPBS with Ca^{2+} and Mg^{2+} (Gibco). Hydrogels were mixed as described above and performed with identical mass and diameter (6 mm) using agarose 2 % (*w/v*) molds. Release studies were performed simulating an 8-day cell culture in a humidified atmosphere at 37 °C and 5 % CO_2. Aliquots consisting of the total amount of immersing liquid (1 mL) were removed from the plates after diverse time points. The reaction of the B present in the collected aliquots with azomethine (Sigma) in an acid medium (KAc/HAc buffer pH 5.2) originates a colorimetric reaction measured at 405 nm in a Victor III (Perkin Elmer) device. Standards for calibration were prepared at concentrations of 0, 0.1, 0.25, 0.5, 1, 1.5, 2.5, 5, 10, 25, 50, and 500 mg mL^{-1} of B, using 40 μL aliquots from the original standard solutions for colorimetric reactions.

4.1.3. Rheometry

Cylindrical hydrogels were prepared by crosslinking the alginate in 9 mm diameter agarose molds. After crosslinking, alginate hydrogels were stored at 4 °C until measured. Rheological experiments were performed on a strain-controlled Discovery HR-2 rheometer (TA Instruments) at 4 °C. Hydrogels were placed between two parallel plates of non-porous stainless steel. The gap between the plates was adjusted using a normal force of 0.1 N to prevent slippage. Temperature was controlled by a Peltier module. First, the range of strain amplitudes for which hydrogels exhibit linear viscoelastic behavior was determined. A dynamic strain sweep, with amplitudes ranging between 0.01 % and 100 %, at the frequency of 1 Hz was implemented. The dynamic shear modulus as a function of the strain was recorded. Second, a dynamic frequency sweep was applied to determine the dependence of the shear storage modulus (G') and loss modulus (G'') on frequency. The frequency varied from 0.01 Hz and 100 Hz at the selected strain of 1 % in the linear region. Five replicates per sample were measured.

4.1.4. Cytotoxicity assay

MTS quantitative assay (The CellTiter 96 Aqueous One Solution Cell Proliferation Assay, Promega) was performed to assess cytocompatibility of ALG and ALG-B injectable hydrogels in direct contact with myotubes. 20,000 cells cm^{-2} were seeded onto a p-24 multi-well plate under differentiation conditions (low serum 2 % FBS for inducing differentiation conditions). Once myotubes were formed (after 4 days), hydrogels were deposited on top of myotubes after gelation and immersed in the culture media for 48 h. Myotubes were then incubated for 3 h with MTS (tetrazolium salt) at 37 °C and the formation of formazan was followed by measuring absorbance at 490 nm. All measurements were performed in triplicate.

4.2. In vivo SOD1 mouse model

The experimental studies with the SOD1 mice model have been conducted according to Spanish and European regulations on the use and treatment of animals (RD 223/88, RD 53/2013, and 10/13/89 OM) and the ETS-123 European Convention on the protection/welfare of vertebrate mammals used in research. Specific authorization for the procedures was obtained (permit number 2020/VSC/PEA/0182), by the Animal Experiment Committee at Universitat Politècnica de València to ensure the avoidance of unnecessary distress, pain, harm, or suffering.

The experimental mice were housed under 12 h light / dark cycles at 23–25 °C with a relative humidity of 55 %. Food and water were available *ad libitum*. Animals were sacrificed by CO_2 inhalation.

100 μL of injectable B-loaded ALG-based hydrogels (ALG—B, 6 mg of B/injection) were subcutaneously injected in both quadriceps muscles at 68, 82, 96, and 110 days old *B6SJL-Tg(SOD1-G93A)1Gur/J* ALS mice. Two different experiments were performed in parallel, differing in their endpoint: i) mice were sacrificed at 115 days old for muscle and nerve

evaluation and ii) mice were sacrificed at their final endpoint determined as the mouse's inability to flip over within 30 s in the supine position (ranging between 120 and 146 days) for evaluation of survival (SV).

For the first experiment, three different groups of male and female mice equally distributed were evaluated: 6 animals (3 males and 3 females) injected with 100 μL of saline solution as an ALS control, 6 animals (3 males and 3 females) with empty ALG hydrogels, and 6 animals (3 males and 3 females) with ALG-B hydrogels. For the survival experiment (SV), two different groups of male and female mice equally distributed were evaluated: 10 animals (5 males and 5 females) injected with 100 μL of saline solution as an ALS control and 10 animals (5 males and 5 females) with ALG-B hydrogels. Note that in order to accomplish with the 3 R's principle the control group ALG is not duplicated in the SV experiment, since ALS and ALG groups generate equivalent results.

Changes in the body weight and motor impairment in the behavioral four-limb hanging test have been followed during the total duration of the experiments in all animals following Treat-NMD Neuromuscular Network Standard Operation Procedures (SOP, treat-nmd.org).

After euthanasia, different tissues were extracted:

- Both muscle quadriceps were removed and immediately fixed in cold isopentane (−150° to −160 °C) (PanReac Applichem) for 1 min, and subsequently immersed in liquid nitrogen for 2 min. Samples were stored at −80 °C until sectioning.
- We ensured comprehensive measurement coverage of the mouse spinal cord by employing a meticulous dissection protocol that encompassed the entirety of the spinal column. Following euthanasia, the mouse was carefully dissected to expose the vertebral column, allowing for precise identification and extraction of the entire spinal cord. The complete spinal cord was removed from vertebrae and immediately fixed in formaldehyde 4 % for 24 h at 4 °C, followed by cryopreservation in 30 % sucrose. Segments from all spinal cord regions (cervical, thoracic, lumbar, and sacral) were meticulously segmented and included in a freezing compound (OCT), and further stored at −80 °C until sectioning.

4.3. Histology and staining

Frozen muscle and spinal cord samples were sectioned using a cryostat at −25/30 °C. 10–15 μm sections were placed on polarized slides (Superfrost, Thermofisher). Muscle histoarchitecture was evaluated by Hematoxylin-eosin staining. Muscle inflammation and motor neuron identification were determined by toluidine blue staining (1 % in saturated borax). All staining was performed following standard procedures. After sample dehydration with graded ethanol series and clearing with xylene, they were mounted with a xylene-based mounting medium (Entellan, Electron Microscopy Sciences). Images were captured with a bright-field microscope (Nikon Eclipse 80i) at different magnifications.

4.4. Immunofluorescence assays

Immunofluorescence assays were performed using cryopreserved slides containing sectioned samples that were air-dry for 15 min at room temperature. Samples were then permeabilized with DPBS/0.5 % Triton x-100 at room temperature for 5 min, next blocked in 2 % BSA/DPBS for 1 h at 37 °C. Samples were then incubated with primary antibodies (Table 1) diluted in a blocking buffer overnight at 4 °C. The samples were then rinsed twice in DPBS/0.1 % Triton X-100 and incubated with the secondary antibody (Table 2) at room temperature for 1 h. Finally, samples were washed twice in DPBS/0.1 % Triton X-100 before mounting with Vectashield containing DAPI (Vector Laboratories) and images were captured under an epifluorescence microscope (Nikon Eclipse 80i) at different magnifications.

Table 1
Primary antibodies used for immunofluorescence assays.

Target	Brand	Reference	Dilution
FN	Sigma-Aldrich	F0916	1:100
GFAP	Abcam	ab7260	1:5000
IL-6	ThermoFisher	P620	1:200
PAX7	Invitrogen	PA1–117	1:200
Slow Skeletal Myosin Heavy Chain	Abcam	Ab234431	1:200
SOD1	Abcam	Ab51254	1:200
TGFβ	Bioss antibodies	bs-0086R	1:100
NGFR (CD271)	Invitrogen	MA5–31968	1:100

Table 2
Secondary antibodies used for immunofluorescence assays.

Target	Brand	Reference	Dilution
Alexa Fluor 488 anti-mouse	Invitrogen	A-11029	1:700
Alexa Fluor 555 anti-rabbit	Invitrogen	A-21428	1:700
Alexa Fluor 555 anti-chicken	Invitrogen	A-21437	1:700

4.5. Gene expression analysis

Total RNA was extracted following the manufacturer's instructions and under RNase-free conditions. Quadriceps muscle tissue (100 mg) from the different animal groups (ALS, ALG, ALG—B) was homogenized in 1 mL TRIZOL (Fisher Scientific) solution using a tissue Homogenizer 850 (Fisher) following 40 s cycles at 18.000 rpm. RNA quantity and integrity were measured with a NanoDrop 1000 (ThermoScientific). Then 2–5 μg of RNA were reverse transcribed using the Superscript III reverse transcriptase (Invitrogen) and oligo dT primer (Invitrogen). Real-time qPCR was performed using Sybr select master mix and 7500 Real-Time PCR system from Applied Biosystems. The reactions were run in triplicate for technical replicas while biological replicas were 6 mice in the case of pre-symptomatic animals and 10 mice in the case of symptomatic animals. The primers used for amplification were designed from sequences found in the GenBank database and are indicated in Table 3.

Table 3
Primer sequences are used for gene expression analysis.

Gene	Primer Sequence
Integrin α_5 (Gene ID: 16402)	Fw: 5′- ACCTGGACCAAGACGGCTACAA-3′ Rev: 5′- CTGGGAAGGTTTAGTGCTCAGTC-3′
Integrin α7 (Gene ID: 16404)	Fw: 5′-TCTGTCAGAGCAACCTCCAGCT-3′ Rev: 5′- CTATGAACGGCTGCCCACTCAA-3′
Integrin αv (Gene ID: 16410)	Fw: 5′- GTGTGAGGAACTGGTCGCCTAT-3′ Rev: 5′- CCGTTCTCTGGTCCAACCGATA-3′
Integrin β1 (Gene ID: 16412)	Fw: 5′- CTCCAGAAGGTGGCTTTGATGC-3′ Rev: 5′-GTGAAACCCAGCATCCGTGGAA-3′
Integrin β3 (Gene ID: 16416)	Fw: 5′-GTGAGTGCGATGACTTCTCCTG-3′ Rev: 5′-CAGGTGTCAGTGCGTGTAGTAC-3′
NaBC1 (Gene ID: 269356)	Fw: 5′-GAGGTTCGCTTTGTCATCCTGG-3′ Rev: 5′-ATGCCAGTGAGCTTCCCGTTCAG-3′
IGF1 (Gene ID: 16000)	Fw: 5′-GTGGATGCTCTTCAGTTCGTGTG-3′ Rev: 5′-TCCAGTCTCCTCAGATCACAGC-3′
IGFR (Gene ID: 16001)	Fw: 5′- CGGGATCTCATCAGCTTCACAG-3′ Rev: 5′-TCCTTGTTCGGAGGCAGGTCTA-3′
AKT (Gene ID: 11651)	Fw: 5′-GGACTACTTGCACTCCGAGAAG-3′ Rev: 5′-CATAGTGGCACCGTCCTTGATC-3′
mTOR (Gene ID: 56717)	Fw: 5′-AGAAGGGTCTCCAAGGACGACT-3′ Rev: 5′-GCAGGACACAAAGGCAGCATTG-3′
MyoD: (Gene ID: 17927)	Fw: 5′-GCACTACAGTGGCGACTCAGAT-3′ Rev: 5′-TAGTAGGCGGTGTCGTAGCCAT-3′
Myogenin (Gene ID: 17928)	Fw: 5′-CCATCCAGTACATTGAGCGCCT-3′ Rev: 5′-CTGTGGGAGTTGCATTCACTGG-3′
GADPH (Gene ID: 14433)	Fw: 5′-CATCACTGCCACCCAGAAGACTG-3′ Rev: 5′-ATGCCAGTGAGCTTCCCGTTCAG-3′

4.6. Image analysis

Muscle sequential images obtained after staining were stitched (Image Composite Editor) and segmented using Cellpose 2.0 a generalist algorithm for segmentation, allowing the identification of cell boundaries and the analysis of all fibers of a muscle cross-section (2000–5000 fibers). This method for analyzing the entire muscle guarantees unbiased results. Muscle histological features were identified manually and quantified using image analysis software ImageJ following Treat-NMD Neuromuscular Network Standard Operation Procedures (SOP, treat-nmd.org). For fiber size determination we have employed the Feret's diameter of muscle fibers cross-sections. This is a robust morphometric parameter that avoids experimental errors related to fiber orientation and sectioning angle. Moreover, it reliably discriminates between dystrophic and normal phenotypes.

4.6.1. Immunofluorescence image analysis

Immunofluorescence staining intensity and area measurements were quantified using Fiji (ImageJ) software. [79] Protein expression levels of SOD1, FN, IL-6, TGFβ, NGFR, and GFAP were analyzed following a previously published protocol. Background subtraction was applied using the sliding paraboloid method with a rolling ball radius of 50 to enhance signal detection.

For spinal cord analysis, the white matter area was manually outlined and quantified in Fiji. A Gaussian blur filter (sigma = 2) was applied to smooth the image, followed by thresholding to define the region of interest. Threshold levels were adjusted manually to accurately capture the full extent of the white matter.

4.7. Statistics and reproducibility

For statistical analysis GraphPad Prism 8.0.2 has been used. Data were reported as mean ± standard deviation. Normal distribution of the data was established using the D'Agostino Pearson omnibus test. Results were analyzed by one-way ANOVA test with Tukey's multiple comparison test ($p = 0.05$) when 3 or more groups were compared. Pairs of samples were compared using unpaired *t*-tests, applying Welch's correction when necessary. A 95 % confidence level was considered significant and is indicated by (*) $p < 0.05$, (**) $p < 0.01$, (***) $p < 0.001$, and (****) $p < 0.0001$.

The survival time of mice was evaluated by producing Kaplan-Meier survival curves. Comparisons of the survival curves were evaluated by Log-rank (Mantel-Cox) test.

CRediT authorship contribution statement

Ana Rodriguez-Romano: Methodology, Investigation. **Juan Gonzalez-Valdivieso:** Methodology, Investigation. **Laura Moreno-Martinez:** Investigation. **Juan Francisco Vázquez Costa:** Supervision, Methodology. **Rosario Osta:** Supervision, Methodology. **Patricia Rico:** Writing – original draft, Supervision, Methodology, Investigation, Funding acquisition, Conceptualization.

Declaration of competing interest

The authors declare that they have no known competing financial interests or personal relationships that could have appeared to influence the work reported in this paper.

Acknowledgments

Funding: PR acknowledges support by grant PID2021-126012OB-I00 funded by MCIN/AEI/10.13039/501100011033/ and by ERDF a way of making Europe, and by CIBER (CB06/01/1026). JGV acknowledges the funding from the European Union-NextGenerationEU and ARISTOS (European Union's Horizon Europe research and innovation programme under the MSCA grant agreement 101081334) programs. PR acknowledges gratefully the charitable funding provided by the ALS patient LEP and her family and the help provided by CGR, JVH, and PMN.

Appendix A. Supplementary data

Supplementary data to this article can be found online at https://doi.org/10.1016/j.ijbiomac.2025.145645.

Data availability

All the original data related to this article are accessible upon request from the corresponding author.

References

[1] J. Riancho, M. Delgado-Alvarado, M.D. Andreu, L. Paz-Fajardo, S. Arozamena, F. J. Gil-Bea, A. López de Munaín, Amyotrophic lateral sclerosis (ALS), cancer, autoimmunity and metabolic disorders: an unsolved tantalizing challenge, Br. J. Pharmacol. 178 (2021) 1269–1278, https://doi.org/10.1111/bph.15151.
[2] P. Masrori, P. Van Damme, Amyotrophic lateral sclerosis: a clinical review, Eur. J. Neurol. 27 (2020) 1918–1929, https://doi.org/10.1111/ene.14393.
[3] S. Penco, C. Lunetta, L. Mosca, E. Maestri, F. Avemaria, C. Tarlarini, M.C. Patrosso, A. Marocchi, M. Corbo, Phenotypic heterogeneity in a SOD1 G93D Italian ALS family: an example of human model to study a complex disease, J. Mol. Neurosci. MN 44 (2011) 25–30, https://doi.org/10.1007/s12031-010-9480-4.
[4] L. Régal, L. Vanopdenbosch, P. Tilkin, L. Van Den Bosch, V. Thijs, R. Sciot, W. Robberecht, The G93C mutation in superoxide dismutase 1: Clinicopathologic phenotype and prognosis, Arch. Neurol. 63 (2006) 262–267, https://doi.org/10.1001/archneur.63.2.262.
[5] J. Lee, S.J. Hyeon, H. Im, H. Ryu, Y. Kim, H. Ryu, Astrocytes and microglia as non-cell autonomous players in the pathogenesis of ALS, Exp. Neurobiol. 25 (2016) 233–240, https://doi.org/10.5607/en.2016.25.5.233.
[6] K.K. Chand, K.M. Lee, J.D. Lee, H. Qiu, E.F. Willis, N.A. Lavidis, M.A. Hilliard, P. G. Noakes, Defects in synaptic transmission at the neuromuscular junction precede motor deficits in a TDP-43Q331K transgenic mouse model of amyotrophic lateral sclerosis, FASEB J. 32 (2018) 2676–2689, https://doi.org/10.1096/fj.201700835R.
[7] E.B. Moloney, F. de Winter, J. Verhaagen, ALS as a distal axonopathy: molecular mechanisms affecting neuromuscular junction stability in the presymptomatic stages of the disease, Front. Neurosci. 8 (2014) 252, https://doi.org/10.3389/fnins.2014.00252.
[8] C. Tallon, K.A. Russell, S. Sakhalkar, N. Andrapallayal, M.H. Farah, Length-dependent axo-terminal degeneration at the neuromuscular synapses of type II muscle in SOD1 mice, Neuroscience 312 (2016) 179–189, https://doi.org/10.1016/j.neuroscience.2015.11.018.
[9] O. Pikatza-Menoio, A. Elicegui, X. Bengoetxea, N. Naldaiz-Gastesi, A. López de Munain, G. Gerenu, F.J. Gil-Bea, S. Alonso-Martín, The skeletal muscle emerges as a new disease target in amyotrophic lateral sclerosis, J. Pers. Med. 11 (2021) 671, https://doi.org/10.3390/jpm11070671.
[10] F. Gouel, A.-S. Rolland, J.-C. Devedjian, T. Burnouf, D. Devos, Past and future of neurotrophic growth factors therapies in ALS: from single neurotrophic growth factor to stem cells and human platelet lysates, Front. Neurol. 10 (2019), https://doi.org/10.3389/fneur.2019.00835.
[11] G. Dobrowolny, C. Giacinti, L. Pelosi, C. Nicoletti, N. Winn, L. Barberi, M. Molinaro, N. Rosenthal, A. Musarò, Muscle expression of a local Igf-1 isoform protects motor neurons in an ALS mouse model, J. Cell Biol. 168 (2005) 193–199, https://doi.org/10.1083/jcb.200407021.
[12] M. Suzuki, J. McHugh, C. Tork, B. Shelley, A. Hayes, I. Bellantuono, P. Aebischer, C.N. Svendsen, Direct muscle delivery of GDNF with human mesenchymal stem cells improves motor neuron survival and function in a rat model of familial ALS, Mol. Ther. J. Am. Soc. Gene Ther. 16 (2008) 2002–2010, https://doi.org/10.1038/mt.2008.197.
[13] D. Krakora, P. Mulcrone, M. Meyer, C. Lewis, K. Bernau, G. Gowing, C. Zimprich, P. Aebischer, C.N. Svendsen, M. Suzuki, Synergistic effects of GDNF and VEGF on lifespan and disease progression in a familial ALS rat model, Mol. Ther. 21 (2013) 1602–1610, https://doi.org/10.1038/mt.2013.108.
[14] T. Amna, M. Shamshi Hassan, M.S. Khil, H.K. Lee, I.H. Hwang, Electrospun nanofibers of ZnO-TiO2 hybrid: characterization and potential as an extracellular scaffold for supporting myoblasts, Surf. Interface Anal. 46 (2014) 72–76, https://doi.org/10.1002/sia.5350.
[15] R. Chhabra, B. Ruozi, A. Vilella, D. Belletti, K. Mangus, S. Pfaender, T. Sarowar, T. M. Boeckers, M. Zoli, F. Forni, M.A. Vandelli, G. Tosi, A. Martin Grabrucker, Application of polymeric nanoparticles for CNS targeted zinc delivery in vivo, CNS Neurol. Disord. - Drug Targets- CNS Neurol. Disord. 14 (2015) 1041–1053.
[16] M. Murariu, A. Doumbia, L. Bonnaud, A.-L. Dechief, Y. Paint, M. Ferreira, C. Campagne, E. Devaux, P. Dubois, High-performance polylactide/ZnO nanocomposites designed for films and fibers with special end-use properties, Biomacromolecules 12 (2011) 1762–1771, https://doi.org/10.1021/bm2001445.
[17] H. Oliveira, S. Catros, C. Boiziau, R. Siadous, J. Marti-Munoz, R. Bareille, S. Rey, O. Castano, J. Planell, J. Amédée, E. Engel, The proangiogenic potential of a novel

calcium releasing biomaterial: impact on cell recruitment, Acta Biomater. 29 (2016) 435–445, https://doi.org/10.1016/j.actbio.2015.10.003.
[18] J.M. Aizpurua, J.I. Miranda, A. Irastorza, E. Torres, M. Eceiza, M. Sagartzazu-Aizpurua, P. Ferrón, G. Aldanondo, H. Lasa-Fernández, P. Marco-Moreno, N. Dadie, A. López de Munain, A. Vallejo-Illarramendi, Discovery of a novel family of FKBP12 "reshapers" and their use as calcium modulators in skeletal muscle under nitro-oxidative stress, Eur. J. Med. Chem. 213 (2021) 113160, https://doi.org/10.1016/j.ejmech.2021.113160.
[19] A. Vallejo-Illarramendi, I. Toral-Ojeda, G. Aldanondo, A. López de Munain, Dysregulation of calcium homeostasis in muscular dystrophies, Expert Rev. Mol. Med. 16 (2014) e16, https://doi.org/10.1017/erm.2014.17.
[20] F. Nielsen, Other trace elements, Present Knowl, Nutr, 1990.
[21] F.H. Nielsen, J.G. Penland, Boron supplementation of peri-menopausal women affects boron metabolism and indices associated with macromineral metabolism, hormonal status and immune function, J. Trace Elem. Exp. Med. 12 (1999) 251–261, https://doi.org/10.1002/(SICI)1520-670X(1999)12:3<251::AID-JTRA8>3.0.CO;2-I.
[22] M. Park, Q. Li, N. Shcheynikov, W. Zeng, S. Muallem, NaBC1 is a ubiquitous electrogenic Na+ −coupled borate transporter essential for cellular boron homeostasis and cell growth and proliferation, Mol. Cell 16 (2004) 331–341, https://doi.org/10.1016/j.molcel.2004.09.030.
[23] J. Gonzalez-Valdivieso, G. Ciccone, U. Dhawan, T. Quon, E. Barcelona-Estaje, A. Rodrigo-Navarro, R.R. Castillo, G. Milligan, P. Rico, M. Salmeron-Sanchez, NaBC1 boron transporter enables myoblast response to substrate rigidity via fibronectin-binding Integrins, Adv. Sci. Weinh. Baden-Wurtt. Ger. (2025) e2407548, https://doi.org/10.1002/advs.202407548.
[24] P. Rico, A. Rodrigo-Navarro, M. de la Peña, V. Moulisová, M. Costell, M. Salmerón-Sánchez, Simultaneous boron Ion-Channel/growth factor receptor activation for enhanced vascularization, Adv. Biosyst. 3 (2019) 1800220, https://doi.org/10.1002/adbi.201800220.
[25] P. Rico, A. Rodrigo-Navarro, L. Sánchez Pérez, M. Salmeron-Sanchez, Borax induces osteogenesis by stimulating NaBC1 transporter via activation of BMP pathway, Commun. Biol. 3 (2020) 1–15, https://doi.org/10.1038/s42003-020-01449-4.
[26] J. Ciriza, A. Rodríguez-Romano, I. Nogueroles, G. Gallego-Ferrer, R.M. Cabezuelo, J.L. Pedraz, P. Rico, Borax-loaded injectable alginate hydrogels promote muscle regeneration in vivo after an injury, Mater. Sci. Eng., C 123 (2021) 112003, https://doi.org/10.1016/j.msec.2021.112003.
[27] P. Rico, A. Rodrigo-Navarro, M. Salmerón-Sánchez, Borax-loaded PLLA for promotion of myogenic differentiation, Tissue Eng. Part A 21 (2015) 2662–2672, https://doi.org/10.1089/ten.tea.2015.0044.
[28] M. Dadon-Nachum, E. Melamed, D. Offen, The "dying-back" phenomenon of motor neurons in ALS, J. Mol. Neurosci. MN 43 (2011) 470–477, https://doi.org/10.1007/s12031-010-9467-1.
[29] S. OLIVÁN, A.C. CALVO, A. RANDO, M.J. MUÑOZ, P. ZARAGOZA, R. OSTA, Comparative study of behavioural tests in the SOD1G93A mouse model of amyotrophic lateral sclerosis, Exp. Anim. 64 (2015) 147–153, https://doi.org/10.1538/expanim.14-0077.
[30] J.D. Atkin, R.L. Scott, J.M. West, E. Lopes, A.K.J. Quah, S.S. Cheema, Properties of slow- and fast-twitch muscle fibres in a mouse model of amyotrophic lateral sclerosis, Neuromuscul. Disord. 15 (2005) 377–388, https://doi.org/10.1016/j.nmd.2005.02.005.
[31] L. Jensen, L.H. Jørgensen, R.D. Bech, U. Frandsen, H.D. Schrøder, Skeletal muscle Remodelling as a function of disease progression in amyotrophic lateral sclerosis, Biomed. Res. Int. 2016 (2016) e5930621, https://doi.org/10.1155/2016/5930621.
[32] H. Westerblad, J.D. Bruton, A. Katz, Skeletal muscle: energy metabolism, fiber types, fatigue and adaptability, Exp. Cell Res. 316 (2010) 3093–3099, https://doi.org/10.1016/j.yexcr.2010.05.019.
[33] P.-F. Pradat, A. Barani, J. Wanschitz, O. Dubourg, A. Lombès, A. Bigot, V. Mouly, G. Bruneteau, F. Salachas, T. Lenglet, V. Meininger, G. Butler-Browne, Abnormalities of satellite cells function in amyotrophic lateral sclerosis, Amyotroph, Lateral Scler. Off. Publ. World Fed. Neurol. Res. Group Mot. Neuron Dis. 12 (2011) 264–271, https://doi.org/10.3109/17482968.2011.566618.
[34] A. Scaramozza, V. Marchese, V. Papa, R. Salaroli, G. Sorarù, C. Angelini, G. Cenacchi, Skeletal muscle satellite cells in amyotrophic lateral sclerosis, Ultrastruct. Pathol. 38 (2014) 295–302, https://doi.org/10.3109/01913123.2014.937842.
[35] S. Tsitkanou, P.A. Della Gatta, A.P. Russell, Skeletal muscle satellite cells, mitochondria, and MicroRNAs: their involvement in the pathogenesis of ALS, Front. Physiol. 7 (2016) 403, https://doi.org/10.3389/fphys.2016.00403.
[36] R. Manzano, J.M. Toivonen, A.C. Calvo, S. Oliván, P. Zaragoza, C. Rodellar, D. Montarras, R. Osta, Altered in vitro proliferation of mouse SOD1-G93A skeletal muscle satellite cells, Neurodegener Dis 11 (2012) 153–164, https://doi.org/10.1159/000338061.
[37] R. Manzano, J.M. Toivonen, A.C. Calvo, S. Oliván, P. Zaragoza, M.J. Muñoz, D. Montarras, R. Osta, Quantity and activation of Myofiber-associated satellite cells in a mouse model of amyotrophic lateral sclerosis, Stem Cell Rev. Rep. 8 (2012) 279–287, https://doi.org/10.1007/s12015-011-9268-0.
[38] M.E. Gurney, H. Pu, A.Y. Chiu, M.C. Dal Canto, C.Y. Polchow, D.D. Alexander, J. Caliendo, A. Hentati, Y.W. Kwon, H.X. Deng, Motor neuron degeneration in mice that express a human Cu,Zn superoxide dismutase mutation, Science 264 (1994) 1772–1775, https://doi.org/10.1126/science.8209258.
[39] M.B. Yim, J.H. Kang, H.S. Yim, H.S. Kwak, P.B. Chock, E.R. Stadtman, A gain-of-function of an amyotrophic lateral sclerosis-associated Cu,Zn-superoxide dismutase mutant: An enhancement of free radical formation due to a decrease in Km for hydrogen peroxide, Proc. Natl. Acad. Sci. U. S. A. 93 (1996) 5709–5714, https://doi.org/10.1073/pnas.93.12.5709.
[40] G. Dobrowolny, M. Aucello, E. Rizzuto, S. Beccafico, C. Mammucari, S. Boncompagni, S. Belia, F. Wannenes, C. Nicoletti, Z. Del Prete, N. Rosenthal, M. Molinaro, F. Protasi, G. Fanò, M. Sandri, A. Musarò, Skeletal muscle is a primary target of SOD1G93A-mediated toxicity, Cell Metab. 8 (2008) 425–436, https://doi.org/10.1016/j.cmet.2008.09.002.
[41] S. Peters, E. Zitzelsperger, S. Kuespert, S. Iberl, R. Heydn, S. Johannesen, S. Petri, L. Aigner, D.R. Thal, A. Hermann, J.H. Weishaupt, T.-H. Bruun, U. Bogdahn, The TGF-β system as a potential pathogenic player in disease modulation of amyotrophic lateral sclerosis, Front. Neurol. 8 (2017) articles/10.3389/fneur.2017.00669.
[42] D. Gonzalez, O. Contreras, D.L. Rebolledo, J.P. Espinoza, B. van Zundert, E. Brandan, ALS skeletal muscle shows enhanced TGF-β signaling, fibrosis and induction of fibro/adipogenic progenitor markers, PLoS One 12 (2017) e0177649, https://doi.org/10.1371/journal.pone.0177649.
[43] I.M. Chiu, H. Phatnani, M. Kuligowski, J.C. Tapia, M.A. Carrasco, M. Zhang, T. Maniatis, M.C. Carroll, Activation of innate and humoral immunity in the peripheral nervous system of ALS transgenic mice, Proc. Natl. Acad. Sci. U. S. A. 106 (2009) 20960–20965, https://doi.org/10.1073/pnas.0911405106.
[44] E. Trias, S. Ibarburu, R. Barreto-Núñez, V. Varela, I.C. Moura, P. Dubreuil, O. Hermine, J.S. Beckman, L. Barbeito, Evidence for mast cells contributing to neuromuscular pathology in an inherited model of ALS, JCI Insight 2 (2017), https://doi.org/10.1172/jci.insight.95934 e95934, 95934.
[45] J.P. Abonia, D.S. Friend, W.G. Austen, F.D. Moore, M.C. Carroll, R. Chan, J. Afnan, A. Humbles, C. Gerard, P. Knight, Y. Kanaoka, S. Yasuda, N. Morokawa, K. F. Austen, R.L. Stevens, M.F. Gurish, Mast cell protease 5 mediates ischemia-reperfusion injury of mouse skeletal muscle, J. Immunol. Baltim. Md 1950 (174) (2005) 7285–7291.
[46] K. Ashina, Y. Tsubosaka, T. Nakamura, K. Omori, K. Kobayashi, M. Hori, H. Ozaki, T. Murata, Histamine induces vascular Hyperpermeability by increasing blood flow and endothelial barrier disruption in vivo, PLoS One 10 (2015) e0132367, https://doi.org/10.1371/journal.pone.0132367.
[47] A.L. Christy, M.E. Walker, M.J. Hessner, M.A. Brown, Mast cell activation and neutrophil recruitment promotes early and robust inflammation in the meninges in EAE, J. Autoimmun. 42 (2013) 50–61, https://doi.org/10.1016/j.jaut.2012.11.003.
[48] S. Wernersson, G. Pejler, Mast cell secretory granules: armed for battle, Nat. Rev. Immunol. 14 (2014) 478–494, https://doi.org/10.1038/nri3690.
[49] M. Schmelz, S. Zeck, M. Raithel, R. Rukwied, Mast cell tryptase in dermal neurogenic inflammation, Clin. Exp. Allergy J. Br. Soc. Allergy Clin. Immunol. 29 (1999) 695–702, https://doi.org/10.1046/j.1365-2222.1999.00514.x.
[50] E. Trias, M. Kovacs, P.H. King, Y. Si, Y. Kwon, V. Varela, S. Ibarburu, I.C. Moura, O. Hermine, J.S. Beckman, L. Barbeito, Schwann cells orchestrate peripheral nerve inflammation through the expression of CSF1, IL-34 and SCF in amyotrophic lateral sclerosis, Glia 68 (2020) 1165–1181, https://doi.org/10.1002/glia.23768.
[51] E. Trias, P.H. King, Y. Si, Y. Kwon, V. Varela, S. Ibarburu, M. Kovacs, I.C. Moura, J. S. Beckman, O. Hermine, L. Barbeito, Mast cells and neutrophils mediate peripheral motor pathway degeneration in ALS, JCI Insight 3 (2018), https://doi.org/10.1172/jci.insight.123249 e123249, 123249.
[52] T. Tanaka, M. Narazaki, T. Kishimoto, IL-6 in inflammation, immunity, and disease, Cold Spring Harbor Perspect. Biol. 6 (2014) a016295, https://doi.org/10.1101/cshperspect.a016295.
[53] C. Brandt, B.K. Pedersen, The role of exercise-induced myokines in muscle homeostasis and the defense against chronic diseases, J. Biomed. Biotechnol. 2010 (2010) 520258, https://doi.org/10.1155/2010/520258.
[54] A. Pronto-Laborinho, S. Pinto, M. Gromicho, M. Pereira, M. Swash, M. de Carvalho, Interleukin-6 and amyotrophic lateral sclerosis, J. Neurol. Sci. 398 (2019) 50–53, https://doi.org/10.1016/j.jns.2019.01.026.
[55] M. Wosiski-Kuhn, J.B. Caress, M.S. Cartwright, G.A. Hawkins, C. Milligan, Interleukin 6 (IL6) level is a biomarker for functional disease progression within IL6R358Ala variant groups in amyotrophic lateral sclerosis patients, Amyotroph. Lateral Scler. Front. Degener. 22 (2021) 248–259, https://doi.org/10.1080/21678421.2020.1813310.
[56] D. Jaarsma, E. Teuling, E.D. Haasdijk, C.I.D. Zeeuw, C.C. Hoogenraad, Neuron-specific expression of mutant superoxide dismutase is sufficient to induce amyotrophic lateral sclerosis in transgenic mice, J. Neurosci. 28 (2008) 2075–2088, https://doi.org/10.1523/JNEUROSCI.5258-07.2008.
[57] J.M. Van Dyke, I.M. Smit-Oistad, C. Macrander, D. Krakora, M.G. Meyer, M. Suzuki, Macrophage-mediated inflammation and glial response in the skeletal muscle of a rat model of familial amyotrophic lateral sclerosis (ALS), Exp. Neurol. 277 (2016) 275–282, https://doi.org/10.1016/j.expneurol.2016.01.008.
[58] F. Bruno, P. Abondio, A. Montesanto, D. Luiselli, A.C. Bruni, R. Maletta, The nerve growth factor receptor (NGFR/p75NTR): a major player in Alzheimer's disease, Int. J. Mol. Sci. 24 (2023) 3200, https://doi.org/10.3390/ijms24043200.
[59] M.E. Alexianu, M. Kozovska, S.H. Appel, Immune reactivity in a mouse model of familial ALS correlates with disease progression, Neurology 57 (2001) 1282–1289, https://doi.org/10.1212/wnl.57.7.1282.
[60] Y. Yoshii, A. Otomo, L. Pan, M. Ohtsuka, S. Hadano, Loss of glial fibrillary acidic protein marginally accelerates disease progression in a SOD1H46R transgenic mouse model of ALS, Neurosci. Res. 70 (2011) 321–329, https://doi.org/10.1016/j.neures.2011.03.006.
[61] M. Hu, Z. Ling, X. Ren, Extracellular matrix dynamics: tracking in biological systems and their implications, J. Biol. Eng. 16 (2022) 13, https://doi.org/10.1186/s13036-022-00292-x.

[62] W. Zhang, Y. Liu, H. Zhang, Extracellular matrix: an important regulator of cell functions and skeletal muscle development, Cell Biosci. 11 (2021) 65, https://doi.org/10.1186/s13578-021-00579-4.
[63] Y.X. Wang, N.A. Dumont, M.A. Rudnicki, Muscle stem cells at a glance, J. Cell Sci. 127 (2014) 4543–4548, https://doi.org/10.1242/jcs.151209.
[64] D. Taverna, M.H. Disatnik, H. Rayburn, R.T. Bronson, J. Yang, T.A. Rando, R. O. Hynes, Dystrophic muscle in mice chimeric for expression of alpha5 integrin, J. Cell Biol. 143 (1998) 849–859, https://doi.org/10.1083/jcb.143.3.849.
[65] H. Liu, A. Niu, S.-E. Chen, Y.-P. Li, Beta3-integrin mediates satellite cell differentiation in regenerating mouse muscle, FASEB, J. Off. Publ. Fed. Am. Soc. Exp. Biol. 25 (2011) 1914–1921, https://doi.org/10.1096/fj.10-170449.
[66] G. Fu, W. Wang, B.-H. Luo, Overview: structural biology of integrins, Methods Mol. Biol. Clifton NJ 757 (2012) 81–99, https://doi.org/10.1007/978-1-61779-166-6_7.
[67] D. Gullberg, T. Velling, L. Lohikangas, C.F. Tiger, Integrins during muscle development and in muscular dystrophies, Front. Biosci. J. Virtual Libr. 3 (1998) D1039–D1050, https://doi.org/10.2741/a344.
[68] M.D. Boppart, Z.S. Mahmassani, Integrin signaling: linking mechanical stimulation to skeletal muscle hypertrophy, Am. J. Physiol. Cell Physiol. 317 (2019) C629–C641, https://doi.org/10.1152/ajpcell.00009.2019.
[69] J.L. Marshall, E. Chou, J. Oh, A. Kwok, D.J. Burkin, R.H. Crosbie-Watson, Dystrophin and utrophin expression require sarcospan: loss of α7 integrin exacerbates a newly discovered muscle phenotype in sarcospan-null mice, Hum. Mol. Genet. 21 (2012) 4378–4393, https://doi.org/10.1093/hmg/dds271.
[70] C. Guo, M. Willem, A. Werner, G. Raivich, M. Emerson, L. Neyses, U. Mayer, Absence of alpha 7 integrin in dystrophin-deficient mice causes a myopathy similar to Duchenne muscular dystrophy, Hum. Mol. Genet. 15 (2006) 989–998, https://doi.org/10.1093/hmg/ddl018.
[71] J. Liu, D.J. Burkin, S.J. Kaufman, Increasing alpha 7 beta 1-integrin promotes muscle cell proliferation, adhesion, and resistance to apoptosis without changing gene expression, Am. J. Physiol. Cell Physiol. 294 (2008) C627–C640, https://doi.org/10.1152/ajpcell.00329.2007.
[72] A. Chiot, S.F. Roemer, L. Ryner, A. Bogachuk, K. Emberley, D. Brownell, G. A. Jimenez, M. Leviten, R. Woltjer, D.W. Dickson, L. Steinman, B. Ajami, Elevated α5 integrin expression on myeloid cells in motor areas in amyotrophic lateral sclerosis is a therapeutic target, Proc. Natl. Acad. Sci. U. S. A. 120 (2023) e2306731120, https://doi.org/10.1073/pnas.2306731120.
[73] M. Laplante, D.M. Sabatini, mTOR signaling in growth control and disease, Cell 149 (2012) 274–293, https://doi.org/10.1016/j.cell.2012.03.017.
[74] G.Y. Liu, D.M. Sabatini, mTOR at the nexus of nutrition, growth, ageing and disease, Nat. Rev. Mol. Cell Biol. 21 (2020) 183–203, https://doi.org/10.1038/s41580-019-0199-y.
[75] M. González-Muñoz, A.I. Rodríguez-Mahillo, C. Gil, Y. Morán, I. Moneo, A. Martínez, J.S. Mora, Glycogen synthase kinase-3β expression and phosphorylation in peripheral blood mononuclear cells of patients with amyotrophic lateral sclerosis, J. Adv. Med. Med. Res. (2014) 263–271, https://doi.org/10.9734/BJMMR/2014/5578.
[76] R. Manzano, J.M. Toivonen, L. Moreno-Martínez, M. de la Torre, L. Moreno-García, T. López-Royo, N. Molina, P. Zaragoza, A.C. Calvo, R. Osta, What skeletal muscle has to say in amyotrophic lateral sclerosis: implications for therapy, Br. J. Pharmacol. 178 (2021) 1279–1297, https://doi.org/10.1111/bph.15276.
[77] J.A. Kim, Y.H. Shon, J.O. Lim, J.J. Yoo, H.-I. Shin, E.K. Park, MYOD mediates skeletal myogenic differentiation of human amniotic fluid stem cells and regeneration of muscle injury, Stem Cell Res. Ther. 4 (2013) 147, https://doi.org/10.1186/scrt358.
[78] Myogenin is an essential regulator of adult myofibre growth and muscle stem cell homeostasis | eLife. https://elifesciences.org/articles/60445, 2023.
[79] J. Schindelin, I. Arganda-Carreras, E. Frise, V. Kaynig, M. Longair, T. Pietzsch, S. Preibisch, C. Rueden, S. Saalfeld, B. Schmid, J.-Y. Tinevez, D.J. White, V. Hartenstein, K. Eliceiri, P. Tomancak, A. Cardona, Fiji: an open-source platform for biological-image analysis, Nat. Methods 9 (2012) 676–682, https://doi.org/10.1038/nmeth.2019.